

Which Training Methods for GANs do actually Converge?

Lars Mescheder¹ Andreas Geiger^{1,2} Sebastian Nowozin³

Abstract

Recent work has shown local convergence of GAN training for absolutely continuous data and generator distributions. In this paper, we show that the requirement of absolute continuity is necessary: we describe a simple yet prototypical counterexample showing that in the more realistic case of distributions that are not absolutely continuous, unregularized GAN training is not always convergent. Furthermore, we discuss regularization strategies that were recently proposed to stabilize GAN training. Our analysis shows that GAN training with instance noise or zero-centered gradient penalties converges. On the other hand, we show that Wasserstein-GANs and WGAN-GP with a finite number of discriminator updates per generator update do not always converge to the equilibrium point. We discuss these results, leading us to a new explanation for the stability problems of GAN training. Based on our analysis, we extend our convergence results to more general GANs and prove local convergence for simplified gradient penalties even if the generator and data distributions lie on lower dimensional manifolds. We find these penalties to work well in practice and use them to learn high-resolution generative image models for a variety of datasets with little hyperparameter tuning.

1. Introduction

Generative Adversarial Networks (GANs) (Goodfellow et al., 2014) are powerful latent variable models that can be used to learn complex real-world distributions. Especially for images, GANs have emerged as one of the dominant approaches for generating new realistically looking samples after the model has been trained on some dataset.

¹MPI Tübingen, Germany ²ETH Zürich, Switzerland

³Microsoft Research, Cambridge, UK. Correspondence to: Lars Mescheder <lars.mescheder@tue.mpg.de>.

Proceedings of the 35th International Conference on Machine Learning, Stockholm, Sweden, PMLR 80, 2018. Copyright 2018 by the author(s).

Method	Local convergence (a.c. case)	Local convergence (general case)
unregularized (Goodfellow et al., 2014)	✓	✗
WGAN (Arjovsky et al., 2017)	✗	✗
WGAN-GP (Gulrajani et al., 2017)	✗	✗
DRAGAN (Kodali et al., 2017)	✓	✗
Instance noise (Sønderby et al., 2016)	✓	✓
ConOpt (Mescheder et al., 2017)	✓	✓
Gradient penalties (Roth et al., 2017)	✓	✓
Gradient penalty on real data only	✓	✓
Gradient penalty on fake data only	✓	✓

Table 1. Convergence properties of different GAN training algorithms for general GAN-architectures. Here, we distinguish between the case where both the data and generator distributions are absolutely continuous (a.c.) and the general case where they may lie on lower dimensional manifolds.

However, while very powerful, GANs can be hard to train and in practice it is often observed that gradient descent based GAN optimization does not lead to convergence. As a result, a lot of recent research has focused on finding better training algorithms (Arjovsky et al., 2017; Gulrajani et al., 2017; Kodali et al., 2017; Sønderby et al., 2016; Roth et al., 2017) for GANs as well as gaining better theoretically understanding of their training dynamics (Arjovsky et al., 2017; Arjovsky & Bottou, 2017; Mescheder et al., 2017; Nagarajan & Kolter, 2017; Heusel et al., 2017).

Despite practical advances, the training dynamics of GANs are still not completely understood. Recently, Mescheder et al. (2017) and Nagarajan & Kolter (2017) showed that local convergence and stability properties of GAN training can be analyzed by examining the eigenvalues of the Jacobian of the the associated gradient vector field: if the Jacobian has only eigenvalues with negative real-part at the equilibrium point, GAN training converges locally for small enough learning rates. On the other hand, if the Jacobian has eigenvalues on the imaginary axis, it is generally not locally convergent. Moreover, Mescheder et al. (2017) showed that if there are eigenvalues close but not on the imaginary axis, the training algorithm can require intractably small learning rates to achieve convergence. While Mescheder et al. (2017) observed eigenvalues close to the imaginary axis in practice, this observation does not answer the question if eigenvalues close to the imaginary axis are a general phenomenon and if yes, whether they are indeed the root cause for the training

instabilities that people observe in practice.

A partial answer to this question was given by [Nagarajan & Kolter \(2017\)](#), who showed that for absolutely continuous data and generator distributions¹ all eigenvalues of the Jacobian have negative real-part. As a result, GANs are locally convergent for small enough learning rates in this case. However, the assumption of absolute continuity is not true for common use cases of GANs, where both distributions may lie on lower dimensional manifolds ([Sønderby et al., 2016](#); [Arjovsky & Bottou, 2017](#)).

In this paper we show that this assumption is indeed necessary: by considering a simple yet prototypical example of GAN training we analytically show that (unregularized) GAN training is not always locally convergent. We also discuss how recent techniques for stabilizing GAN training affect local convergence on our example problem. Our findings show that neither Wasserstein GANs (WGANs) ([Arjovsky et al., 2017](#)) nor Wasserstein GANs with Gradient Penalty (WGAN-GP) ([Gulrajani et al., 2017](#)) nor DRAGAN ([Kodali et al., 2017](#)) converge on this simple example for a fixed number of discriminator updates per generator update. On the other hand, we show that instance noise ([Sønderby et al., 2016](#); [Arjovsky & Bottou, 2017](#)), zero-centered gradient penalties ([Roth et al., 2017](#)) and consensus optimization ([Mescheder et al., 2017](#)) lead to local convergence.

Based on our analysis, we give a new explanation for the instabilities commonly observed when training GANs based on discriminator gradients orthogonal to the tangent space of the data manifold. We also introduce simplified gradient penalties for which we prove local convergence. We find that these gradient penalties work well in practice, allowing us to learn high-resolution image based generative models for a variety of datasets with little hyperparameter tuning.

In summary, our contributions are as follows:

- We identify a simple yet prototypical counterexample showing that (unregularized) gradient descent based GAN optimization is not always locally convergent
- We discuss if and how recently introduced regularization techniques stabilize the training
- We introduce simplified gradient penalties and prove local convergence for the regularized GAN training dynamics

All proofs can be found in the supplementary material.

¹[Nagarajan & Kolter \(2017\)](#) also proved local convergence for a slightly more general family of probability distributions where the support of the generator distribution is equal to the support of the true data distribution near the equilibrium point. Alternatively, they showed that their results also hold when the discriminator satisfies certain (strong) smoothness conditions. However, these conditions are usually hard to satisfy in practice without prior knowledge about the support of the true data distribution.

2. Instabilities in GAN training

2.1. Background

GANs are defined by a min-max two-player game between a discriminative network $D_\psi(x)$ and generative network $G_\theta(z)$. While the discriminator tries to distinguish between real data point and data points produced by the generator, the generator tries to fool the discriminator. It can be shown ([Goodfellow et al., 2014](#)) that if both the generator and discriminator are powerful enough to approximate any real-valued function, the unique Nash-equilibrium of this two player game is given by a generator that produces the true data distribution and a discriminator which is 0 everywhere on the data distribution.

Following the notation of [Nagarajan & Kolter \(2017\)](#), the training objective for the two players can be described by an objective function of the form

$$L(\theta, \psi) = E_{p(z)} [f(D_\psi(G_\theta(z)))] + E_{p_D(x)} [f(-D_\psi(x))] \quad (1)$$

for some real-valued function f . The common choice $f(t) = -\log(1 + \exp(-t))$ leads to the loss function considered in the original GAN paper ([Goodfellow et al., 2014](#)). For technical reasons we assume that f is continuously differentiable and satisfies $f'(t) \neq 0$ for all $t \in \mathbb{R}$.

The goal of the generator is to minimize this loss whereas the discriminator tries to maximize it. Our goal when training GANs is to find a Nash-equilibrium, i.e. a parameter assignment (θ^*, ψ^*) where neither the discriminator nor the generator can improve their utilities unilaterally.

GANs are usually trained using Simultaneous or Alternating Gradient Descent (SimGD and AltGD). Both algorithms can be described as fixed point algorithms ([Mescheder et al., 2017](#)) that apply some operator $F_h(\theta, \psi)$ to the parameter values (θ, ψ) of the generator and discriminator, respectively. For example, simultaneous gradient descent corresponds to the operator $F_h(\theta, \psi) = (\theta, \psi) + h v(\theta, \psi)$, where $v(\theta, \psi)$ denotes the *gradient vector field*

$$v(\theta, \psi) := \begin{pmatrix} -\nabla_\theta L(\theta, \psi) \\ \nabla_\psi L(\theta, \psi) \end{pmatrix}. \quad (2)$$

Similarly, alternating gradient descent can be described by an operator $F_h = F_{2,h} \circ F_{1,h}$ where $F_{1,h}$ and $F_{2,h}$ perform an update for the generator and discriminator, respectively.

Recently, it was shown ([Mescheder et al., 2017](#)) that local convergence of GAN training near an equilibrium point (θ^*, ψ^*) can be analyzed by looking at the spectrum of the Jacobian $F'_h(\theta^*, \psi^*)$ at the equilibrium: if $F'_h(\theta^*, \psi^*)$ has eigenvalues with absolute value bigger than 1, the training algorithm will generally not converge to (θ^*, ψ^*) . On the other hand, if all eigenvalues have absolute value smaller

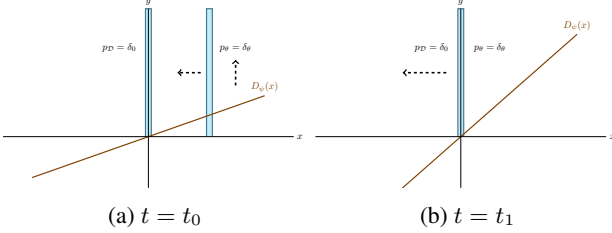


Figure 1. Visualization of the counterexample showing that gradient descent based GAN optimization is not always convergent: (a) In the beginning, the discriminator pushes the generator towards the true data distribution and the discriminator’s slope increases. (b) When the generator reaches the target distribution, the slope of the discriminator is largest, pushing the generator away from the target distribution. This results in oscillatory training dynamics that never converge.

than 1, the training algorithm will converge to (θ^*, ψ^*) with linear rate $\mathcal{O}(|\lambda_{\max}|^k)$ where λ_{\max} is the eigenvalue of $F'(\theta^*, \psi^*)$ with the biggest absolute value. If all eigenvalues of $F'(\theta^*, \psi^*)$ are on the unit circle, the algorithm can be convergent, divergent or neither, but if it is convergent it will generally converge with a sublinear rate. A similar result (Khalil, 1996; Nagarajan & Kolter, 2017) also holds for the (idealized) continuous system

$$\begin{pmatrix} \dot{\theta}(t) \\ \dot{\psi}(t) \end{pmatrix} = \begin{pmatrix} -\nabla_\psi L(\theta, \psi) \\ \nabla_\theta L(\theta, \psi) \end{pmatrix} \quad (3)$$

which corresponds to training the GAN with infinitely small learning rate: if all eigenvalues of the Jacobian $v'(\theta^*, \psi^*)$ at a stationary point (θ^*, ψ^*) have negative real-part, the continuous system converges locally to (θ^*, ψ^*) with linear convergence rate. On the other hand, if $v'(\theta^*, \psi^*)$ has eigenvalues with positive real-part, the continuous system is not locally convergent. If all eigenvalues have zero real-part, it can be convergent, divergent or neither, but if it is convergent, it will generally converge with a sublinear rate.

For simultaneous gradient descent linear convergence can be achieved if and only if all eigenvalues of the Jacobian of the gradient vector field $v(\theta, \psi)$ have negative real part (Mescheder et al., 2017). This situation was also considered by Nagarajan & Kolter (2017) who examined the asymptotic case of step sizes h that go to 0 and proved local convergence for absolutely continuous generator and data distributions under certain regularity assumptions.

2.2. The Dirac-GAN

Simple experiments, simple theorems are the building blocks that help us understand more complicated systems.

Ali Rahimi - Test of Time Award speech, NIPS 2017

In this section, we describe a simple yet prototypical counterexample which shows that in the general case unregularized GAN training is neither locally nor globally convergent.

Definition 2.1. The Dirac-GAN consists of a (univariate) generator distribution $p_\theta = \delta_\theta$ and a linear discriminator $D_\psi(x) = \psi \cdot x$. The true data distribution p_D is given by a Dirac-distribution concentrated at 0.

Note that for the Dirac-GAN, both the generator and the discriminator have exactly one parameter. This situation is visualized in Figure 1. In this setup, the GAN training objective (1) is given by

$$L(\theta, \psi) = f(\psi\theta) + f(0) \quad (4)$$

While using linear discriminators might appear restrictive, the class of linear discriminators is in fact as powerful as the class of all real-valued functions for this example: when we use $f(t) = -\log(1 + \exp(-t))$ and we take the supremum over ψ in (4), we obtain (up to scalar and additive constants) the Jensen-Shannon divergence between p_θ and p_D . The same holds true for the Wasserstein-divergence, when we use $f(t) = t$ and put a Lipschitz constraint on the discriminator (see Section 3.1).

We show that the training dynamics of GANs do not converge in this simple setup.

Lemma 2.2. The unique equilibrium point of the training objective in (4) is given by $\theta = \psi = 0$. Moreover, the Jacobian of the gradient vector field at the equilibrium point has the two eigenvalues $\pm f'(0)$ i which are both on the imaginary axis.

We now take a closer look at the training dynamics produced by various algorithms for training the Dirac-GAN. First, we consider the (idealized) continuous system in (3): while Lemma 2.2 shows that the continuous system is generally not linearly convergent to the equilibrium point, it could in principle converge with a sublinear convergence rate. However, this is not the case as the next lemma shows:

Lemma 2.3. The integral curves of the gradient vector field $v(\theta, \psi)$ do not converge to the Nash-equilibrium. More specifically, every integral curve $(\theta(t), \psi(t))$ of the gradient vector field $v(\theta, \psi)$ satisfies $\theta(t)^2 + \psi(t)^2 = \text{const}$ for all $t \in [0, \infty)$.

Note that our results do not contradict the results of Nagarajan & Kolter (2017) and Heusel et al. (2017): our example violates Assumption IV in Nagarajan & Kolter (2017) that the support of the generator distribution is equal to the support of the true data distribution near the equilibrium. It also violates the assumption² in Heusel et al. (2017) that the optimal discriminator parameter vector is a continuous function of the current generator parameters. In fact, unless

²This assumption is usually even violated by Wasserstein-GANs, as the optimal discriminator parameter vector as a function of the current generator parameters can have discontinuities near the Nash-equilibrium. See Section 3.1 for details.

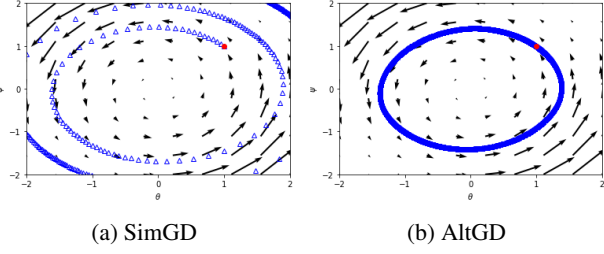


Figure 2. Training behavior of the Dirac-GAN. The starting iterate is marked in red.

$\theta = 0$, there is not even an optimal discriminator parameter for the Dirac-GAN. Indeed, we found that two-time scale updates as suggested by Heusel et al. (2017) do not help convergence towards the Nash-equilibrium (see Figure 22 in the supplementary material). However, our example seems to be a prototypical situation for (unregularized) GAN training which usually deals with distributions that are concentrated on lower dimensional manifolds (Arjovsky & Bottou, 2017).

We now take a closer look at the *discretized system*.

Lemma 2.4. *For simultaneous gradient descent, the Jacobian of the update operator $F_h(\theta, \psi)$ has eigenvalues $\lambda_{1/2} = 1 \pm h f'(0)i$ with absolute values $\sqrt{1 + h^2 f'(0)^2}$ at the Nash-equilibrium. Independently of the learning rate, simultaneous gradient descent is therefore not stable near the equilibrium. Even stronger, for every initial condition and learning rate $h > 0$, the norm of the iterates (θ_k, ψ_k) obtained by simultaneous gradient descent is monotonically increasing.*

The behavior of simultaneous gradient descent for our example problem is visualized in Figure 2a.

Similarly, for alternating gradient descent we have

Lemma 2.5. *For alternating gradient descent with n_g generator and n_d discriminator updates, the Jacobian of the update operator $F_h(\theta, \psi)$ has eigenvalues*

$$\lambda_{1/2} = 1 - \frac{\alpha^2}{2} \pm \sqrt{\left(1 - \frac{\alpha^2}{2}\right)^2 - 1}. \quad (5)$$

with $\alpha := \sqrt{n_g n_d} h f'(0)$. For $\alpha \leq 2$, all eigenvalues are hence on the unit circle. Moreover for $\alpha > 2$, there are eigenvalues outside the unit circle.

Even though Lemma 2.5 shows that alternating gradient descent does not converge linearly to the Nash-equilibrium, it could in principle converge with a sublinear convergence rate. However, this is very unlikely because – as Lemma 2.3 shows – even the continuous system does not converge. Indeed, we empirically found that alternating gradient descent oscillates in stable cycles around the equilibrium and shows no sign of convergence (Figure 2b).

2.3. Where do instabilities come from?

Our simple example shows that naive gradient based GAN optimization does not always converge to the equilibrium point. To get a better understanding of what can go wrong for more complicated GANs, it is instructive to analyze these instabilities in depth for this simple example problem.

To understand the instabilities, we have to take a closer look at the oscillatory behavior that GANs exhibit both for the Dirac-GAN and for more complex systems. An intuitive explanation for the oscillations is given in Figure 1: when the generator is far from the true data distribution, the discriminator pushes the generator towards the true data distribution. At the same time, the discriminator becomes more certain, which increases the discriminator's slope (Figure 1a). Now, when the generator reaches the target distribution (Figure 1b), the slope of the discriminator is largest, pushing the generator away from the target distribution. As a result, the generator moves away again from the true data distribution and the discriminator has to change its slope from positive to negative. After a while, we end up with a similar situation as in the beginning of training, only on the other side of the true data distribution. This process repeats indefinitely and does not converge.

Another way to look at this is to consider the local behavior of the training algorithm near the Nash-equilibrium. Indeed, near the Nash-equilibrium, there is nothing that pushes the discriminator towards having zero slope on the true data distribution. Even if the generator is initialized *exactly* on the target distribution, there is no incentive for the discriminator to move to the equilibrium discriminator. As a result, training is unstable near the equilibrium point.

This phenomenon of discriminator gradients orthogonal to the data distribution can also arise for more complex examples: as long as the data distribution is concentrated on a low dimensional manifold and the class of discriminators is big enough, there is no incentive for the discriminator to produce zero gradients orthogonal to the tangent space of the data manifold and hence converge to the equilibrium discriminator. Even if the generator produces *exactly* the true data distribution, there is no incentive for the discriminator to produce zero gradients orthogonal to the tangent space. When this happens, the discriminator does not provide useful gradients for the generator orthogonal to the data distribution and the generator does not converge.

Note that these instabilities can only arise if the true data distribution is concentrated on a lower dimensional manifold. Indeed, Nagarajan & Kolter (2017) showed that – under some suitable assumptions – gradient descent based GAN optimization is locally convergent for absolutely continuous distributions. Unfortunately, this assumption may not be satisfied for data distributions like natural images to

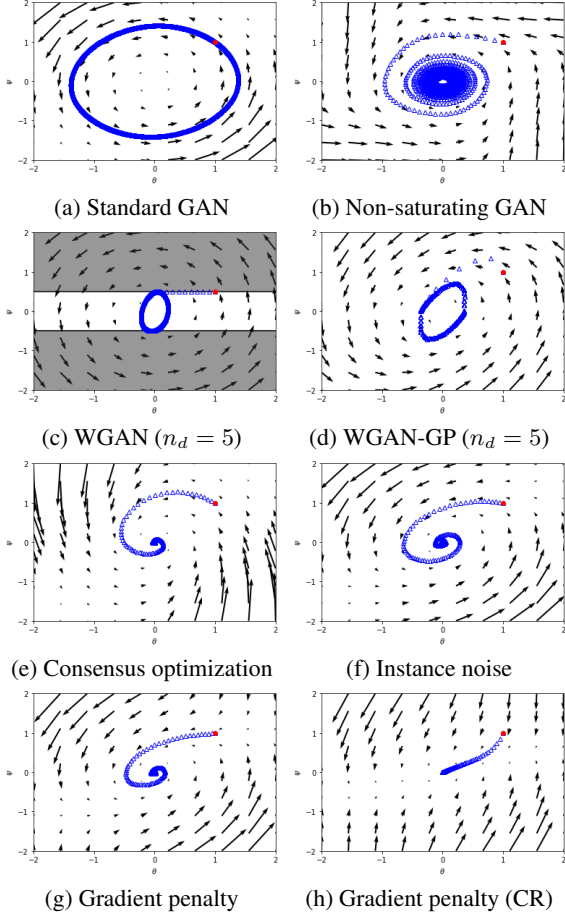


Figure 3. Convergence properties of different GAN training algorithms using alternating gradient descent with recommended number of discriminator updates per generator update ($n_d = 1$ if not noted otherwise). The shaded area in Figure 3c visualizes the set of forbidden values for the discriminator parameter ψ . The starting iterate is marked in red.

which GANs are commonly applied (Arjovsky & Bottou, 2017). Moreover, even if the data distribution is absolutely continuous but concentrated along some lower dimensional manifold, the eigenvalues of the Jacobian of the gradient vector field will be very close to the imaginary axis, resulting in a highly ill-conditioned problem. This was observed by Mescheder et al. (2017) who examined the spectrum of the Jacobian for a data distribution given by a circular mixture of Gaussians with small variance.

3. Regularization strategies

As we have seen in Section 2, unregularized GAN training does not always converge to the Nash-equilibrium. In this section, we discuss how several regularization techniques that have recently been proposed, influence convergence of the Dirac-GAN.

Interestingly, we also find that the non-saturating loss pro-

posed in the original GAN paper (Goodfellow et al., 2014) leads to convergence of the continuous system, albeit with an extremely slow convergence rate. A more detailed discussion and an analysis of consensus optimization (Mescheder et al., 2017) can be found in the supplementary material.

3.1. Wasserstein GAN

The two-player GAN game can be interpreted as minimizing a probabilistic divergence between the true data distribution and the distribution produced by the generator (Nowozin et al., 2016; Goodfellow et al., 2014). This divergence is obtained by considering the best-response strategy for the discriminator, resulting in an objective function that only contains the generator parameters. Many recent regularization techniques for GANs are based on the observation (Arjovsky & Bottou, 2017) that this divergence may be discontinuous with respect to the parameters of the generator or may even take on infinite values if the support of the data distribution and the generator distribution do not match.

To make the divergence continuous with respect to the parameters of the generator, Wasserstein GANs (WGANS) Arjovsky et al. (2017) replace the Jensen-Shannon divergence used in the original derivation of GANs (Goodfellow et al., 2014) with the Wasserstein-divergence. As a result, Arjovsky et al. (2017) propose to use $f(t) = t$ and restrict the class of discriminators to Lipschitz continuous functions with Lipschitz constant equal to some $g_0 > 0$. While a WGAN converges if the discriminator is always trained until convergence, in practice WGANs are usually trained by running only a fixed finite number of discriminator updates per generator update. However, near the Nash-equilibrium the optimal discriminator parameters can have a discontinuity as a function of the current generator parameters: for the Dirac-GAN, the optimal discriminator has to move from $\psi = -1$ to $\psi = 1$ when θ changes signs. As the gradients get smaller near the equilibrium point, the gradient updates do not lead to convergence for the discriminator. Overall, the training dynamics are again determined by the Jacobian of the gradient vector field near the Nash-equilibrium:

Lemma 3.1. *A WGAN trained with simultaneous or alternating gradient descent with a fixed number of discriminator updates per generator update and a fixed learning rate $h > 0$ does generally not converge to the Nash equilibrium for the Dirac-GAN.*

The training behavior of the WGAN is visualized in Figure 3c. We stress that this analysis only holds if the discriminator is trained with a fixed number of discriminator updates (as it is usually done in practice). More careful training that ensures that the discriminator is kept exactly optimal or two-timescale training (Heusel et al., 2017) might be able to ensure convergence for WGANs.

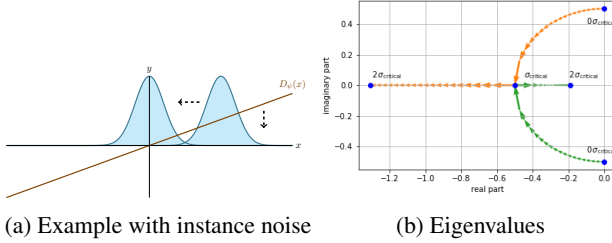


Figure 4. Dirac-GAN with instance noise. While unregularized GAN training is inherently unstable, instance noise can stabilize it: (a) Near the Nash-equilibrium, the discriminator is pushed towards the zero discriminator. (b) As we increase the noise level σ from 0 to σ_{critical} , the real part of the eigenvalues at the equilibrium point becomes negative and the absolute value of the imaginary part becomes smaller. For noise levels bigger than σ_{critical} all eigenvalues are real-valued and GAN training hence behaves like a normal optimization problem.

The convergence properties of WGANs were also considered by Nagarajan & Kolter (2017) who showed that even for absolutely continuous densities and infinitesimal learning rates, WGANs are not always locally convergent.

We also found that WGAN-GP (Gulrajani et al., 2017) does not converge for the Dirac-GAN (Figure 3d). Please see the supplementary material for details.³

3.2. Instance noise

A common technique to stabilize GANs is to add *instance noise* (Sønderby et al., 2016; Arjovsky & Bottou, 2017), i.e. independent Gaussian noise, to the data points. While the original motivation was to make the probabilistic divergence between data and generator distribution well-defined for distributions that do not have common support, this does not clarify the effects of instance noise on the *training algorithm* itself and its ability to find a Nash-equilibrium. Interestingly, however, it was recently shown (Nagarajan & Kolter, 2017) that in the case of absolutely continuous distributions, gradient descent based GAN optimization is - under suitable assumptions - locally convergent.

Indeed, for the Dirac-GAN we have:

Lemma 3.2. *When using Gaussian instance noise with standard deviation σ , the eigenvalues of the Jacobian of the gradient vector field are given by*

$$\lambda_{1/2} = f''(0)\sigma^2 \pm \sqrt{f''(0)^2\sigma^4 - f'(0)^2}. \quad (6)$$

In particular, all eigenvalues of the Jacobian have negative real-part at the Nash-equilibrium if $f''(0) < 0$ and $\sigma > 0$. Hence, simultaneous and alternating gradient descent are both locally convergent for small enough learning rates.

³Despite these negative results, WGAN-GP has been successfully applied in practice (Gulrajani et al., 2017; Karras et al., 2017) and we leave a theoretical analysis of these empirical results to future research.

Interestingly, Lemma 3.2 shows that there is a critical noise level given by $\sigma_{\text{critical}}^2 = |f'(0)|/|f''(0)|$. If the noise level is smaller than the critical noise level, the eigenvalues of the Jacobian have non-zero imaginary part which results in a rotational component in the gradient vector field near the equilibrium point. If the noise level is larger than the critical noise level, all eigenvalues of the Jacobian become real-valued and the rotational component in the gradient vector field disappears. The optimization problem is best behaved when we select $\sigma = \sigma_{\text{critical}}$: in this case we can even achieve quadratic convergence for $h = |f'(0)|^{-1}$. The effect of instance noise on the eigenvalues is visualized in Figure 4b, which shows the traces of the two eigenvalues as we increase σ from 0 to $2\sigma_{\text{critical}}$.

Figure 3f shows the training behavior of the GAN with instance noise, showing that instance noise indeed creates a strong radial component in the gradient vector field which makes the training algorithm converge.

3.3. Zero-centered gradient penalties

Motivated by the success of instance noise to make the f -divergence between two distributions well-defined, Roth et al. (2017) derived a local approximation to instance noise that results in a zero-centered⁴ gradient penalty for the discriminator.

For the Dirac-GAN, a penalty on the squared norm of the gradients of the discriminator (no matter where) results in the regularizer

$$R(\psi) = \frac{\gamma}{2}\psi^2. \quad (7)$$

This regularizer does not include the weighting terms considered by Roth et al. (2017). However, the same analysis can also be applied to the regularizer with the additional weighting, yielding almost exactly the same results (see Section D.2 of the supplementary material).

Lemma 3.3. *The eigenvalues of the Jacobian of the gradient vector field for the gradient-regularized Dirac-GAN at the equilibrium point are given by*

$$\lambda_{1/2} = -\frac{\gamma}{2} \pm \sqrt{\frac{\gamma^2}{4} - f'(0)^2}. \quad (8)$$

In particular, for $\gamma > 0$ all eigenvalues have negative real part. Hence, simultaneous and alternating gradient descent are both locally convergent for small enough learning rates.

Like for instance noise, there is a critical regularization parameter $\gamma_{\text{critical}} = 2|f'(0)|$ that results in a locally rotation free vector field. A visualization of the training behavior of the Dirac-GAN with gradient penalty is shown in Figure 3g. Figure 3h illustrates the training behavior of the GAN with

⁴In contrast to the gradient regularizers used in WGAN-GP and DRAGAN which are not zero-centered.

gradient penalty and critical regularization (CR). In particular, we see that near the Nash-equilibrium the vector field does not have a rotational component anymore and hence behaves like a normal optimization problem.

4. General convergence results

In Section 3 we analyzed the convergence properties of various regularization strategies for the Dirac-GAN. In this section, we consider general GANs. First, we introduce two simplified versions of the zero-centered gradient penalty proposed by Roth et al. (2017). We then show that these gradient penalties allow us to extend the convergence proof by Nagarajan & Kolter (2017) to the case where the generator and data distribution do not locally have the same support.⁵ As a result, our convergence proof for the regularized training dynamics also holds for the more realistic case where both the generator and data distributions may lie on lower dimensional manifolds.

4.1. Simplified gradient penalties

Our analysis suggests that the main effect of the zero-centered gradient penalties proposed by Roth et al. (2017) on local stability is to penalize the discriminator for deviating from the Nash-equilibrium. The simplest way to achieve this is to penalize the gradient on real data alone: when the generator distribution produces the true data distribution and the discriminator is equal to 0 on the data manifold, the gradient penalty ensures that the discriminator cannot create a non-zero gradient orthogonal to the data manifold without suffering a loss in the GAN game.

This leads to the following regularization term:

$$R_1(\psi) := \frac{\gamma}{2} \mathbb{E}_{p_{\mathcal{D}}(x)} [\|\nabla D_{\psi}(x)\|^2]. \quad (9)$$

Note that this regularizer is a simplified version of the regularizer derived by Roth et al. (2017). However, our regularizer does not contain the additional weighting terms and penalizes the discriminator gradients only on the true data distribution.

We also consider a similar regularization term given by

$$R_2(\theta, \psi) := \frac{\gamma}{2} \mathbb{E}_{p_{\theta}(x)} [\|\nabla D_{\psi}(x)\|^2] \quad (10)$$

where we penalize the discriminator gradients on the current generator distribution instead of the true data distribution.

Note that for the Dirac-GAN from Section 2, both regularizers reduce to the gradient penalty from Section 3.3 whose behavior is visualized in Figure 3g and Figure 3h.

⁵ Assumption IV in Nagarajan & Kolter (2017)

4.2. Convergence

In this section we present convergence results for the regularized GAN-training dynamics for both regularization terms $R_1(\psi)$ and $R_2(\psi)$ under some suitable assumptions.⁶

Let (θ^*, ψ^*) denote an equilibrium point of the regularized training dynamics. In our convergence analysis, we consider the realizable case, i.e. we assume that there are generator parameters that make the generator produce the true data distribution:

Assumption I. *We have $p_{\theta^*} = p_{\mathcal{D}}$ and $D_{\psi^*}(x) = 0$ in some local neighborhood of $\text{supp } p_{\mathcal{D}}$.*

Like Nagarajan & Kolter (2017), we assume that f satisfies the following property:

Assumption II. *We have $f'(0) \neq 0$ and $f''(0) < 0$.*

An extension of our convergence proof to $f(t) = t$ (as in WGANs) can be found in the supplementary material.

The convergence proof is complicated by the fact that for neural networks, there generally is not a single equilibrium point (θ^*, ψ^*) , but a submanifold of equivalent equilibria corresponding to different parameterizations of the same function. We therefore define the *reparameterization manifolds* \mathcal{M}_G and \mathcal{M}_D . To this end, let

$$h(\psi) := \mathbb{E}_{p_{\mathcal{D}}(x)} [|D_{\psi}(x)|^2 + \|\nabla_x D_{\psi}(x)\|^2]. \quad (11)$$

The *reparameterization manifolds* are then defined as

$$\mathcal{M}_G := \{\theta \mid p_{\theta} = p_{\mathcal{D}}\} \quad \mathcal{M}_D := \{\psi \mid h(\psi) = 0\}. \quad (12)$$

To prove local convergence, we have to assume some regularity properties for \mathcal{M}_G and \mathcal{M}_D near the equilibrium point. To state these assumptions, we need

$$g(\theta) := \mathbb{E}_{p_{\theta}(x)} [\nabla_{\psi} D_{\psi}(x)|_{\psi=\psi^*}]. \quad (13)$$

Assumption III. *There are ϵ -balls $B_{\epsilon}(\theta^*)$ and $B_{\epsilon}(\psi^*)$ around θ^* and ψ^* so that $\mathcal{M}_G \cap B_{\epsilon}(\theta^*)$ and $\mathcal{M}_D \cap B_{\epsilon}(\psi^*)$ define C^1 -manifolds. Moreover, the following holds:*

- (i) *if $v \in \mathbb{R}^n$ is not in the tangent space of \mathcal{M}_D at ψ^* , then $\partial_v^2 h(\psi^*) \neq 0$.*
- (ii) *if $w \in \mathbb{R}^m$ is not in the tangent space of \mathcal{M}_G at θ^* , then $\partial_w g(\theta^*) \neq 0$.*

While formally similar, the two conditions in Assumption III have very different meanings: the first condition is a simple regularity property that means that the geometry of \mathcal{M}_D can be locally described by the second derivative of h . The second condition implies that the discriminator is strong

⁶ Our results also hold for any convex combination of R_1 and R_2 and the regularizer with the additional weighting terms derived by Roth et al. (2017). See the supplementary material for details.

enough so that it can detect any deviation from the equilibrium generator distribution. Indeed, this is the only point where we assume that the class of representable discriminators is sufficiently expressive (and excludes, for example, the trivial case $D_\psi = 0$ for all ψ).

We are now ready to state our main convergence result. To this end, consider the regularized gradient vector field

$$\tilde{v}_i(\theta, \psi) := \begin{pmatrix} -\nabla_\theta L(\theta, \psi) \\ \nabla_\psi L(\theta, \psi) - \nabla_\psi R_i(\theta, \psi) \end{pmatrix}. \quad (14)$$

Theorem 4.1. Assume Assumption I, II and III hold for (θ^*, ψ^*) . For small enough learning rates, simultaneous and alternating gradient descent for \tilde{v}_1 and \tilde{v}_2 are both convergent to $\mathcal{M}_G \times \mathcal{M}_D$ in a neighborhood of (θ^*, ψ^*) . Moreover, the rate of convergence is at least linear.

Theorem 4.1 shows that GAN training with our gradient penalties is convergent when initialized sufficiently close to the equilibrium point. While this does not show that the method is globally convergent, it at least shows that near the equilibrium the method is well-behaved.

4.3. Stable equilibria for unregularized GAN training

As we have seen in Section 2, unregularized GAN training does not always converge to the Nash-equilibrium. However, this does not rule out the existence of stable equilibria for every GAN architecture. In Section E of the supplementary material, we identify two forms of stable equilibria that may exist for unregularized GAN training (*energy solutions* and *full-rank solutions*). However, it is not yet clear under what conditions such solutions exist for high dimensional data distributions.

5. Experiments

2D-Problems Measuring convergence for GANs is hard for high dimensional problems, because we lack a metric that can reliably detect non-convergent behavior. We therefore first examine the behavior of the different regularizers on simple 2D examples where we can assess convergence using an estimate of the Wasserstein-1-distance.

To this end, we run 5 different training algorithms on 4 different 2D-examples for 6 different GAN architectures. For each method, we try both stochastic gradient descent and RMS-Prop with 4 different learning rates. For the R_1 -, R_2 - and WGAN-GP-regularizers we try 3 different regularization parameters. We train all methods for 50k iterations and report the results for the best hyperparameter setup. Please see the supplementary material for details.

The results are shown in Figure 5. We see that the R_1 - and R_2 -regularizers perform similarly and they achieve slightly better results than unregularized training or training with

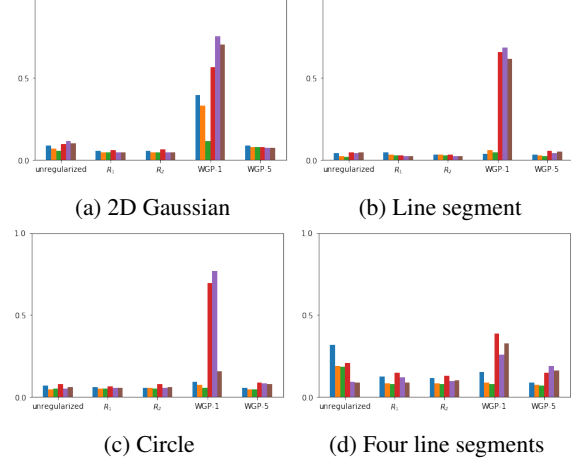


Figure 5. Wasserstein-1-distance to true data distribution for 4 different 2D-data-distributions, 6 different architectures (small bars) and 5 different training methods. Here, we abbreviate WGAN-GP with 1 and 5 discriminator update(s) per generator update as WGP-1 and WGP-5.

WGAN-GP. In the supplementary material we show that the R_1 - and R_2 -regularizers find solutions where the discriminator is 0 in a neighborhood of the true data distribution, whereas unregularized training and WGAN-GP converge to *energy solutions*.

Images To test how well the gradient penalties from Section 4.1 perform on more complicated tasks, we train convolutional GANs on a variety of datasets, including a generative model for all 1000 Imagenet classes and a generative model for the celebA-HQ dataset (Karras et al., 2017) at resolution 1024×1024 . While we find that unregularized GAN training quickly leads to mode-collapse for these problems, our simple R_1 -regularizer enables stable training. Random samples from the models and more details on the experimental setup can be found in the supplementary material.

6. Conclusion

In this paper, we analyzed the stability of GAN training on a simple yet prototypical example. Due to the simplicity of the example, we were able to analyze the convergence properties of the training dynamics analytically and we showed that (unregularized) gradient based GAN optimization is not always locally convergent. Our findings also show that WGANs and WGAN-GP do not always lead to local convergence whereas instance noise and zero-centered gradient penalties do. Based on our analysis, we extended our results to more general GANs and we proved local convergence for simplified zero-centered gradient penalties under suitable assumptions. In the future, we would like to extend our theory to the non-realizable case and examine the effect of finite sampling sizes on the GAN training dynamics.

Acknowledgements

We would like to thank Vaishnavh Nagarajan and Kevin Roth for insightful discussions. We also thank Vaishnavh Nagarajan for giving helpful feedback on an early draft of this manuscript. We thank NVIDIA for donating the GPUs for the experiments presented in the supplementary material. This work was supported by Microsoft Research through its PhD Scholarship Programme.

References

- Abadi, M., Barham, P., Chen, J., Chen, Z., Davis, A., Dean, J., Devin, M., Ghemawat, S., Irving, G., Isard, M., Kudlur, M., Levenberg, J., Monga, R., Moore, S., Murray, D. G., Steiner, B., Tucker, P. A., Vasudevan, V., Warden, P., Wicke, M., Yu, Y., and Zheng, X. Tensorflow: A system for large-scale machine learning. In *12th USENIX Symposium on Operating Systems Design and Implementation, OSDI 2016, Savannah, GA, USA, November 2-4, 2016*, pp. 265–283, 2016.
- Arjovsky, M. and Bottou, L. Towards principled methods for training generative adversarial networks. *CoRR*, abs/1701.04862, 2017.
- Arjovsky, M., Chintala, S., and Bottou, L. Wasserstein GAN. *CoRR*, abs/1701.07875, 2017.
- Barratt, S. and Sharma, R. A note on the inception score. *CoRR*, abs/1801.01973, 2018.
- Berthelot, D., Schumm, T., and Metz, L. BEGAN: boundary equilibrium generative adversarial networks. *CoRR*, abs/1703.10717, 2017.
- Bertsekas, D. P. *Nonlinear programming*. Athena scientific Belmont, 1999.
- Gidel, G., Berard, H., Vincent, P., and Lacoste-Julien, S. A variational inequality perspective on generative adversarial nets. *CoRR*, abs/1802.10551, 2018.
- Goodfellow, I. J., Pouget-Abadie, J., Mirza, M., Xu, B., Warde-Farley, D., Ozair, S., Courville, A. C., and Bengio, Y. Generative adversarial nets. In *Advances in Neural Information Processing Systems 27: Annual Conference on Neural Information Processing Systems 2014, December 8-13 2014, Montreal, Quebec, Canada*, pp. 2672–2680, 2014.
- Gulrajani, I., Ahmed, F., Arjovsky, M., Dumoulin, V., and Courville, A. C. Improved training of wasserstein gans. In *Advances in Neural Information Processing Systems 30: Annual Conference on Neural Information Processing Systems 2017, 4-9 December 2017, Long Beach, CA, USA*, pp. 5769–5779, 2017.
- He, K., Zhang, X., Ren, S., and Sun, J. Deep residual learning for image recognition. In *Proceedings of the IEEE conference on computer vision and pattern recognition*, pp. 770–778, 2016.
- Heusel, M., Ramsauer, H., Unterthiner, T., Nessler, B., and Hochreiter, S. Gans trained by a two time-scale update rule converge to a local nash equilibrium. In *Advances in Neural Information Processing Systems 30: Annual Conference on Neural Information Processing Systems 2017, 4-9 December 2017, Long Beach, CA, USA*, pp. 6629–6640, 2017.
- Hjelm, R. D., Jacob, A. P., Che, T., Cho, K., and Bengio, Y. Boundary-seeking generative adversarial networks. *CoRR*, abs/1702.08431, 2017.
- Karras, T., Aila, T., Laine, S., and Lehtinen, J. Progressive growing of gans for improved quality, stability, and variation. *CoRR*, abs/1710.10196, 2017.
- Khalil, H. K. Nonlinear systems. *Prentice-Hall, New Jersey*, 2(5):5–1, 1996.
- Kodali, N., Abernethy, J. D., Hays, J., and Kira, Z. How to train your DRAGAN. *CoRR*, abs/1705.07215, 2017.
- Krizhevsky, A. and Hinton, G. Learning multiple layers of features from tiny images. 2009.
- Liu, Z., Luo, P., Wang, X., and Tang, X. Deep learning face attributes in the wild. In *Proceedings of International Conference on Computer Vision (ICCV)*, 2015.
- Mescheder, L. M., Nowozin, S., and Geiger, A. The numerics of gans. In *Advances in Neural Information Processing Systems 30: Annual Conference on Neural Information Processing Systems 2017, 4-9 December 2017, Long Beach, CA, USA*, pp. 1823–1833, 2017.
- Miyato, T., Kataoka, T., Koyama, M., and Yoshida, Y. Spectral normalization for generative adversarial networks. *CoRR*, abs/1802.05957, 2018.
- Nagarajan, V. and Kolter, J. Z. Gradient descent GAN optimization is locally stable. In *Advances in Neural Information Processing Systems 30: Annual Conference on Neural Information Processing Systems 2017, 4-9 December 2017, Long Beach, CA, USA*, pp. 5591–5600, 2017.
- Nowozin, S., Cseke, B., and Tomioka, R. f-gan: Training generative neural samplers using variational divergence minimization. In *Advances in Neural Information Processing Systems 29: Annual Conference on Neural Information Processing Systems 2016, December 5-10, 2016, Barcelona, Spain*, pp. 271–279, 2016.

Odena, A., Olah, C., and Shlens, J. Conditional image synthesis with auxiliary classifier gans. In *Proceedings of the 34th International Conference on Machine Learning, ICML 2017, Sydney, NSW, Australia, 6-11 August 2017*, pp. 2642–2651, 2017.

Radford, A., Metz, L., and Chintala, S. Unsupervised representation learning with deep convolutional generative adversarial networks. *CoRR*, abs/1511.06434, 2015.

Roth, K., Lucchi, A., Nowozin, S., and Hofmann, T. Stabilizing training of generative adversarial networks through regularization. In *Advances in Neural Information Processing Systems 30: Annual Conference on Neural Information Processing Systems 2017, 4-9 December 2017, Long Beach, CA, USA*, pp. 2015–2025, 2017.

Russakovsky, O., Deng, J., Su, H., Krause, J., Satheesh, S., Ma, S., Huang, Z., Karpathy, A., Khosla, A., Bernstein, M., Berg, A. C., and Fei-Fei, L. ImageNet Large Scale Visual Recognition Challenge. *International Journal of Computer Vision (IJCV)*, 115(3):211–252, 2015. doi: 10.1007/s11263-015-0816-y.

Salimans, T., Goodfellow, I. J., Zaremba, W., Cheung, V., Radford, A., and Chen, X. Improved techniques for training gans. In *Advances in Neural Information Processing Systems 29: Annual Conference on Neural Information Processing Systems 2016, December 5-10, 2016, Barcelona, Spain*, pp. 2226–2234, 2016.

Sønderby, C. K., Caballero, J., Theis, L., Shi, W., and Huszár, F. Amortised MAP inference for image super-resolution. *CoRR*, abs/1610.04490, 2016.

Tieleman, T. and Hinton, G. Lecture 6.5-rmsprop: Divide the gradient by a running average of its recent magnitude, 2012.

Yazici, Y., Foo, C. S., Winkler, S., Yap, K., Piliouras, G., and Chandrasekhar, V. The unusual effectiveness of averaging in GAN training. *CoRR*, abs/1806.04498, 2018.

Yu, F., Zhang, Y., Song, S., Seff, A., and Xiao, J. LSUN: construction of a large-scale image dataset using deep learning with humans in the loop. *CoRR*, abs/1506.03365, 2015.

Zhao, J. J., Mathieu, M., and LeCun, Y. Energy-based generative adversarial network. *CoRR*, abs/1609.03126, 2016.

Which Training Methods for GANs do actually Converge?

Supplementary Material

A. Preliminaries

In this section we first summarize some results from the theory of discrete dynamical systems. We also prove a discrete version of a basic convergence theorem for continuous dynamical systems from [Nagarajan & Kolter \(2017\)](#) which allows us to make statements about training algorithms for GANs for finite learning rates. Afterwards, we summarize some results from [Mescheder et al. \(2017\)](#) about the convergence properties of simultaneous and alternating gradient descent. Moreover, we state some eigenvalue bounds that were derived by [Nagarajan & Kolter \(2017\)](#) which we need to prove Theorem 4.1 on the convergence of the regularized GAN training dynamics.

A.1. Discrete dynamical systems

In this section, we recall some basic definitions from the theory of discrete nonlinear dynamical systems. For a similar description of the theory of continuous nonlinear dynamical systems see for example [Khalil \(1996\)](#) and [Nagarajan & Kolter \(2017\)](#).

In this paper, we consider continuously differentiable operators $F : \Omega \rightarrow \Omega$ acting on an open set $\Omega \subset \mathbb{R}^n$. A fixed point of F is a point $\bar{x} \in \Omega$ such that $F(\bar{x}) = \bar{x}$. We are interested in stability and convergence of the fixed point iteration $F^{(k)}(x)$ near the fixed point. To this end, we first have to define what we mean by stability and local convergence:

Definition A.1. Let $\bar{x} \in \Omega$ be a fixed point of a continuously differentiable operator $F : \Omega \rightarrow \Omega$. We call \bar{x}

- stable if for every $\epsilon > 0$ there is $\delta > 0$ such that $\|x - \bar{x}\| < \delta$ implies $\|F^{(k)}(x) - \bar{x}\| < \epsilon$ for all $k \in \mathbb{N}$.
- asymptotically stable if it is stable and there is $\delta > 0$ such that $\|x - \bar{x}\| < \delta$ implies that $F^{(k)}(x)$ converges to \bar{x} .
- exponentially stable if there is $\lambda \in [0, 1)$, $\delta > 0$ and $C > 0$ such that $\|x - \bar{x}\| < \delta$ implies

$$\|F^{(k)}(x) - \bar{x}\| < C\|x - \bar{x}\|\lambda^k \quad (15)$$

for all $k \in \mathbb{N}$.

If \bar{x} is asymptotically stable fixed point of F , we call the algorithm obtained by iteratively applying F locally convergent to \bar{x} . If \bar{x} is exponentially stable, we call the cor-

responding algorithm linearly convergent. Moreover, if \bar{x} is exponentially stable, we call the infimum of all λ so that (15) holds for some $C > 0$ the *convergence rate* of the fixed point iteration.

As it turns out, local convergence of fixed point iterations can be analyzed by examining the spectrum of the Jacobian of the fixed point operator. We have the following central Theorem:

Theorem A.2. Let $F : \Omega \rightarrow \Omega$ be a \mathcal{C}^1 -mapping on an open subset Ω of \mathbb{R}^n and $\bar{x} \in \Omega$ be a fixed point of F . Assume that the absolute values of the eigenvalues of the Jacobian $F'(\bar{x})$ are all smaller than 1. Then the fixed point iteration $F^{(k)}(x)$ is locally convergent to \bar{x} . Moreover, the rate of convergence is at least linear with convergence rate $|\lambda_{\max}|$ where λ_{\max} denotes the eigenvalue of $F'(\bar{x})$ with the largest absolute value.

Proof. See [Bertsekas \(1999\)](#), Proposition 4.4.1. \square

For the proof of Theorem 4.1 in Section D, we need a generalization of Theorem A.2 that takes into account submanifolds of fixed points. The next theorem is a discrete version of Theorem A.4 from [Nagarajan & Kolter \(2017\)](#) and we prove it in a similar way:

Theorem A.3. Let $F(\alpha, \gamma)$ define a \mathcal{C}^1 -mapping that maps some domain Ω to itself. Assume that there is a local neighborhood U of 0 such that $F(0, \gamma) = (0, \gamma)$ for $\gamma \in U$. Moreover, assume that all eigenvalues of $J := \nabla_\alpha F(\alpha, 0)|_{\alpha=0}$ have absolute value smaller than 1. Then the fixed point iteration defined by F is locally convergent to $\mathcal{M} := \{(0, \gamma) | \gamma \in U\}$ with linear convergence rate in a neighborhood of $(0, 0)$. Moreover, the convergence rate is $|\lambda_{\max}|$ with λ_{\max} the eigenvalue of J with largest absolute value.

Proof. In the following, we write $F(\alpha, \gamma) = (F_1(\alpha, \gamma), F_2(\alpha, \gamma))$, so that the fixed point iteration can be written as

$$\alpha_{k+1} = F_1(\alpha_k, \gamma_k) \quad \gamma_{k+1} = F_2(\alpha_k, \gamma_k). \quad (16)$$

We first examine the behavior of F_1 near $(0, 0)$. To this end, we develop F_1 into a Taylor-series

$$F_1(\alpha, \gamma) = J\alpha + g_1(\alpha, \gamma) \quad (17)$$

We first show that for any $c > 0$ we have $\|g_1(\alpha, \gamma)\| \leq c\|\alpha\|$ sufficiently close to $(0, 0)$: because $F_1(0, \gamma) = 0$ for all γ close to 0, $g_1(\alpha, \gamma)$ must be of the form $g_1(\alpha, \gamma) = h_1(\alpha, \gamma)\alpha$ with $h_1(0, 0) = 0$. This shows that for any $c > 0$ there is indeed an open neighborhood V of $(0, 0)$ so that $|g_1(\alpha, \gamma)| \leq c\|\alpha\|$ for all $(\alpha, \gamma) \in V$.

According to [Bertsekas \(1999\)](#), Proposition A 15, we can select for every $\epsilon > 0$ a norm $\|\cdot\|_Q$ on \mathbb{R}^n such that

$$\|J\alpha\|_Q < (|\lambda_{\max}| + \epsilon)\|\alpha\|_Q \quad (18)$$

for $\alpha \in \mathbb{R}^n$ where $|\lambda_{\max}|$ denotes the eigenvalue of J with the largest absolute value.

Hence, for $(\alpha, \gamma) \in V$,

$$\begin{aligned} \|F_1(\alpha, \gamma)\|_Q &\leq \|J\alpha\|_Q + \|g_1(\alpha, \gamma)\|_Q \\ &< (|\lambda_{\max}| + \epsilon + c)\|\alpha\|_Q \end{aligned} \quad (19)$$

Because we can make $c + \epsilon$ as small as we want, this shows that $\|\alpha_k\| \leq C\lambda^k\|\alpha_0\|$ for some $C > 0$ and $\lambda \in [0, 1)$, if α_0 and all γ_l for $l = 0, \dots, k-1$ are sufficiently close to 0. We therefore have to show that the iterates γ_k stay in a given local neighborhood of 0, i.e. $\|\gamma_k\| < \delta$ for some $\delta > 0$, when α_0 and γ_0 are initialized sufficiently close to 0.

To show this, we develop F_2 into a Taylor-series around 0:

$$F_2(\alpha, \gamma) = \gamma + g_2(\alpha, \gamma). \quad (20)$$

Again, we see that g_2 must be of the form $g_2(\alpha, \gamma) = h_2(\alpha, \gamma)\alpha$, showing that $\|g_2(\alpha, \gamma)\| \leq c'\|\alpha\|_Q$ for some fixed constant $c' > 0$ (note that in general $h_2(0, 0) \neq 0$). We therefore have

$$\begin{aligned} \|\gamma_k - \gamma_0\| &\leq \sum_{l=0}^{k-1} \|g_2(\alpha_l, \gamma_l)\| \leq \sum_{l=0}^{k-1} c'\|\alpha_l\|_Q \\ &\leq \sum_{l=0}^{k-1} Cc'\lambda^l\|\alpha_0\|_Q \leq \frac{Cc'}{1-\lambda}\|\alpha_0\|_Q \end{aligned} \quad (21)$$

Hence, if we initialize α_0 within $\|\alpha_0\|_Q < \frac{1-\lambda}{2Cc'}\delta$ and γ_0 within $\|\gamma_0\| < \frac{\delta}{2}$, we have $\|\gamma_k\| < \delta$ for all $k \in \mathbb{N}$, concluding the proof. \square

A.2. Simultaneous and Alternating Gradient Descent

In this section, we recall some results from [Mescheder et al. \(2017\)](#) about the convergence properties of simultaneous and alternating gradient descent as algorithms for training generative adversarial networks.

Recall that simultaneous gradient descent can be described by an update operator of the form

$$F_h(\theta, \psi) = \begin{pmatrix} \theta - h\nabla_\theta L(\theta, \psi) \\ \psi + h\nabla_\psi L(\theta, \psi) \end{pmatrix} \quad (22)$$

where $L(\theta, \psi)$ is the GAN training objective defined in (1).

Similarly, alternating gradient descent can be described by an update operator of the form $F_h = F_{2,h} \circ F_{1,h}$ where $F_{1,h}$ and $F_{2,h}$ are given by

$$F_{1,h}(\theta, \psi) = \begin{pmatrix} \theta - h\nabla_\theta L(\theta, \psi) \\ \psi \end{pmatrix} \quad (23)$$

$$F_{2,h}(\theta, \psi) = \begin{pmatrix} \theta \\ \psi + h\nabla_\psi L(\theta, \psi) \end{pmatrix}. \quad (24)$$

Moreover, we defined the gradient vector field

$$v(\theta, \psi) = \begin{pmatrix} -\nabla_\theta L(\theta, \psi) \\ \nabla_\psi L(\theta, \psi) \end{pmatrix}. \quad (25)$$

To understand convergence of simultaneous and alternating gradient descent, we have to understand when the Jacobian of the corresponding update operator has only eigenvalues with absolute value smaller than 1.

Lemma A.4. *The eigenvalues of the Jacobian of the update operator for simultaneous gradient descent are given by $\lambda = 1 + h\mu$ with μ the eigenvalues of $v'(\theta^*, \psi^*)$. Assume that $v'(\theta^*, \psi^*)$ has only eigenvalues with negative real part. The eigenvalues of the Jacobian of the update operator F_h for simultaneous gradient descent are then all in the unit circle if and only if*

$$h < \frac{1}{|\operatorname{Re}(\lambda)|} \frac{2}{1 + \left(\frac{\operatorname{Im}(\lambda)}{\operatorname{Re}(\lambda)}\right)^2} \quad (26)$$

for all eigenvalues λ of $v'(\theta^*, \psi^*)$.

Proof. For simultaneous gradient descent we have

$$F_h(\theta, \psi) = (\theta, \psi) + hv(\theta, \psi) \quad (27)$$

and hence $F'_h(\theta^*, \psi^*) = I + hv'(\theta^*, \psi^*)$. Therefore the eigenvalues are given by $\lambda = 1 + h\mu$ with μ the eigenvalues of $v'(\theta^*, \psi^*)$.

To see when $|\lambda| < 1$, we write $\mu = -a + ib$ with $a, b \in \mathbb{R}$ and $a > 0$. Then

$$|\lambda|^2 = (1 - ha)^2 + h^2b^2 \quad (28)$$

which is smaller than 1 if and only if

$$h < \frac{2a}{a^2 + b^2}. \quad (29)$$

Dividing both the numerator and denominator by a^2 shows the assertion. \square

Lemma A.5. *Assume that $v'(\theta^*, \psi^*)$ has only eigenvalues with negative real part. For $h > 0$ small enough, the eigenvalues of the Jacobian of the update operator F_h for alternating gradient descent are then all in the unit circle.*

Proof. The Jacobian of the update operator $F_h = F_{h,2} \circ F_{h,1}$ at an equilibrium point (θ^*, ψ^*) is

$$F'_h(\theta^*, \psi^*) = F'_{h,2}(\theta^*, \psi^*) \cdot F'_{h,1}(\theta^*, \psi^*). \quad (30)$$

However, we have

$$F'_{h,i}(\theta^*, \psi^*) = I + hv'_i(\theta^*, \psi^*) \quad (31)$$

for $i \in \{1, 2\}$ where

$$v_1(\theta, \psi) = \begin{pmatrix} -\nabla_\theta L(\theta, \psi) \\ 0 \end{pmatrix} \quad (32)$$

$$v_2(\theta, \psi) = \begin{pmatrix} 0 \\ \nabla_\psi L(\theta, \psi) \end{pmatrix} \quad (33)$$

denote the components of the gradient vector field. Hence

$$\begin{aligned} F'_h(\theta^*, \psi^*) &= I + h(v'_1(\theta^*, \psi^*) + v'_2(\theta^*, \psi^*)) \\ &\quad + h^2 v'_2(\theta^*, \psi^*) v'_1(\theta^*, \psi^*) \\ &= I + h(v'(\theta^*, \psi^*) + hR(\theta^*, \psi^*)). \end{aligned} \quad (34)$$

with $R(\theta^*, \psi^*) := v'_2(\theta^*, \psi^*) v'_1(\theta^*, \psi^*)$. For $h > 0$ small enough, all eigenvalues of $v'(\theta^*, \psi^*) + hR(\theta^*, \psi^*)$ will be arbitrarily close to the eigenvalues of $v'(\theta^*, \psi^*)$. Because all eigenvalues of $v'(\theta^*, \psi^*)$ have negative real-part, all eigenvalues of $F'_h(\theta^*, \psi^*)$ will hence lie inside the unit circle for $h > 0$ small enough. \square

In the proof of Theorem 4.1 we will use local coordinates, i.e. a diffeomorphism ϕ that maps a local neighborhood of (θ^*, ψ^*) to an open subset of \mathbb{R}^{n+m} . The vector field v and the update operator F_h then have the following representation in the local coordinates:

$$F_h^\phi(\alpha) := \phi \circ F_h \circ \phi^{-1}(\alpha) \quad (35)$$

$$v^\phi(\alpha) = \phi'(\theta, \psi) \cdot (v \circ \phi^{-1}(\alpha)) \quad (36)$$

While in local coordinates, the simple relationships between $F_h^\phi(\alpha)$ and $v^\phi(\alpha)$ needed to prove Lemma A.4 and Lemma A.5 do not hold anymore, the spectrum can be described in the same way:

Remark A.6. Assume (θ^*, ψ^*) is a fixed point of F_h and a stationary point of v . Let $\alpha^* = \phi(\theta^*, \psi^*)$. Then

$$(F_h^\phi)'(\alpha^*) = \phi'(\theta^*, \psi^*) F'_h(\theta^*, \psi^*) \phi'(\theta^*, \psi^*)^{-1} \quad (37)$$

$$(v^\phi)'(\alpha^*) = \phi'(\theta^*, \psi^*) v'(\theta^*, \psi^*) \phi'(\theta^*, \psi^*)^{-1} \quad (38)$$

Hence, $(F_h^\phi)'(\alpha^*)$ and $F'_h(\theta^*, \psi^*)$ have the same spectrum. The same also holds for $(v^\phi)'(\alpha^*)$ and $v'(\theta^*, \psi^*)$.

Proof. This follows from the chain and product rules by using the fact that $F_h(\theta^*, \psi^*) = (\theta^*, \psi^*)$ and $v(\theta^*, \psi^*) = 0$. \square

As we will see in the proof of Theorem 4.1, Remark A.6 allows us to apply Theorem A.3 to situations where the stationary points lie on a lower dimensional manifold instead of a space of the form $\{0\}^k \times \mathbb{R}^{n+m-k}$.

A.3. Eigenvalue bounds

When analyzing the convergence properties of GANs, we have to analyze the spectrum of real-valued matrices of the form

$$\begin{pmatrix} 0 & -B^\top \\ B & -Q \end{pmatrix} \quad (39)$$

with Q symmetric positive definite. To this end, we need the following important theorem from [Nagarajan & Kolter \(2017\)](#) which gives explicit bounds on the real part of the eigenvalues:

Theorem A.7. Assume $J \in \mathbb{R}^{(n+m) \times (n+m)}$ is of the following form:

$$J = \begin{pmatrix} 0 & -B^\top \\ B & -Q \end{pmatrix} \quad (40)$$

where $Q \in \mathbb{R}^{m \times m}$ is a symmetric positive definite matrix and $B \in \mathbb{R}^{m \times n}$ has full column rank. Then all eigenvalues λ of J satisfy $\text{Re}(\lambda) < 0$. More precisely

- if $\text{Im}(\lambda) = 0$

$$\text{Re}(\lambda) \leq -\frac{\lambda_{\min}(Q)\lambda_{\min}(B^\top B)}{\lambda_{\max}(Q)\lambda_{\min}(Q) + \lambda_{\min}(B^\top B)} \quad (41)$$

- if $\text{Im}(\lambda) \neq 0$

$$\text{Re}(\lambda) \leq -\frac{\lambda_{\min}(Q)}{2} \quad (42)$$

Proof. See [Nagarajan & Kolter \(2017\)](#), Lemma G.2. \square

In Section E.1, we need a generalization of Theorem A.7. Using almost exactly the same proof as for Theorem A.7, we obtain

Theorem A.8. Assume $J \in \mathbb{R}^{(n+m) \times (n+m)}$ is of the following form:

$$J = \begin{pmatrix} -P & -B^\top \\ B & -Q \end{pmatrix} \quad (43)$$

where $P \in \mathbb{R}^{n \times n}$ is a symmetric positive semi-definite matrix, $Q \in \mathbb{R}^{m \times m}$ is a symmetric positive definite matrix and $B \in \mathbb{R}^{m \times n}$ has full column rank. Then all eigenvalues λ of J satisfy $\text{Re}(\lambda) < 0$.

Proof. Let $v^\top = (a^\top, b^\top)$ denote some eigenvector of J with corresponding eigenvalues $\lambda = \lambda_r + i\lambda_i$, where $\lambda_r, \lambda_i \in \mathbb{R}$. Then

$$\lambda_r = \frac{1}{2} \bar{v}^\top (J + J^\top) v = -\bar{a}^\top P a - \bar{b}^\top Q b. \quad (44)$$

Because both P and Q are positive semi-definite, we have $\lambda_r \leq 0$. Because Q is positive definite, it suffices to show that $b \neq 0$ to prove $\lambda_r < 0$.

Assume that $b = 0$. Because v is an eigenvector of J , we have $Ba - Qb = \lambda b$ and therefore $Ba = 0$. Because B has full-column rank, this shows $a = 0$ and hence $v = 0$. However, this contradicts the fact that v is an eigenvector of J . All in all, this shows that $b \neq 0$ and thus $\lambda_r \leq -\bar{b}^\top Qb < 0$ as required. \square

For applying Theorems A.2, we have to show that the Jacobian of the update operator F_h only has eigenvalues with absolute value smaller than 1. For simultaneous and alternating gradient descent this can be achieved (Lemma A.4 and A.5), if the Jacobian of the gradient vector field v only has eigenvalues with negative real-part. While this condition suffices to prove convergence for small learning rates, Mescheder et al. (2017) showed that simultaneous and alternating gradient descent might still require intractably small learning rates if the imaginary part of the eigenvalues is large. However, in our case we have the following simple bound on the imaginary part of the eigenvalues:

Lemma A.9. *Let*

$$J = \begin{pmatrix} -P & -B^\top \\ B & -Q \end{pmatrix} \quad (45)$$

where $P \in \mathbb{R}^{n \times n}$ and $Q \in \mathbb{R}^{m \times m}$ are symmetric. All eigenvalues λ of J then satisfy

$$|\operatorname{Im}(\lambda)| \leq \sqrt{\lambda_{\max}(B^\top B)}. \quad (46)$$

Note that this bound is independent from P and Q .

Proof. Assume v , $\|v\| = 1$, is an eigenvector of J with eigenvalue λ . Then

$$\operatorname{Im}(\lambda) = \bar{v}^\top J_a v. \quad (47)$$

with $J_a := \frac{1}{2i}(J - J^\top)$. Hence, by the Cauchy-Schwarz inequality

$$|\operatorname{Im}(\lambda)| \leq \|v\| \|J_a v\| = \|J_a v\|. \quad (48)$$

But, if $v^\top = (a^\top, b^\top)$,

$$\|J_a v\|^2 = b B B^\top b + a B^\top B a \leq \lambda_{\max}(B^\top B). \quad (49)$$

This shows

$$|\operatorname{Im}(\lambda)| \leq \sqrt{\lambda_{\max}(B^\top B)}. \quad (50)$$

B. Proofs for the Dirac-GAN

This section contains the proofs for our results from Section 2 and Section 3 on the properties of the Dirac-GAN.

Lemma 2.2. *The unique equilibrium point of the training objective in (4) is given by $\theta = \psi = 0$. Moreover, the Jacobian of the gradient vector field at the equilibrium point has the two eigenvalues $\pm f'(0)i$ which are both on the imaginary axis.*

Proof. The loss in (4) can be rewritten as

$$L(\theta, \psi) = f(\theta\psi) + \text{const} \quad (51)$$

It is easy to check that the gradient vector field is given by

$$v(\theta, \psi) = \begin{pmatrix} -f'(\theta\psi)\psi \\ f'(\theta\psi)\theta \end{pmatrix}. \quad (52)$$

Because $L(\theta, 0) = L(0, \psi) = \text{const}$ for all $\theta, \psi \in \mathbb{R}$, $(\theta, \psi) = (0, 0)$ is indeed a Nash-equilibrium for the game defined by (51). Because we assume $f'(t) \neq 0$ for all $t \in \mathbb{R}$, we have $v(\theta, \psi) = 0$ if and only if $(\theta, \psi) = (0, 0)$, showing that $(0, 0)$ is indeed the unique Nash-equilibrium.

Moreover, the Jacobian $v'(\theta, \psi)$ of v is given by

$$\begin{pmatrix} -f''(\theta\psi)\psi^2 & -f'(\theta\psi) - f''(\theta\psi)\theta\psi \\ f'(\theta\psi) + f''(\theta\psi)\theta\psi & f''(\theta\psi)\theta^2 \end{pmatrix}. \quad (53)$$

Evaluating it at the Nash equilibrium $\theta = \psi = 0$, we obtain

$$v'(0, 0) = \begin{pmatrix} 0 & -f'(0) \\ f'(0) & 0 \end{pmatrix} \quad (54)$$

which has the eigenvalues $\pm f'(0)i$. \square

Lemma 2.3. *The integral curves of the gradient vector field $v(\theta, \psi)$ do not converge to the Nash-equilibrium. More specifically, every integral curve $(\theta(t), \psi(t))$ of the gradient vector field $v(\theta, \psi)$ satisfies $\theta(t)^2 + \psi(t)^2 = \text{const}$ for all $t \in [0, \infty)$.*

Proof. Let $R(\theta, \psi) := \frac{1}{2}(\theta^2 + \psi^2)$. Then

$$\begin{aligned} \frac{d}{dt} R(\theta(t), \psi(t)) \\ = \theta(t)v_1(\theta(t), \psi(t)) + \psi(t)v_2(\theta(t), \psi(t)) = 0, \end{aligned} \quad (55)$$

showing that $R(\theta, \psi)$ is indeed constant for all $t \in [0, \infty)$. \square

Lemma 2.4. *For simultaneous gradient descent, the Jacobian of the update operator $F_h(\theta, \psi)$ has eigenvalues $\lambda_{1/2} = 1 \pm h f'(0)i$ with absolute values $\sqrt{1 + h^2 f'(0)^2}$ at the Nash-equilibrium. Independently of the learning rate, simultaneous gradient descent is therefore not stable near*

the equilibrium. Even stronger, for every initial condition and learning rate $h > 0$, the norm of the iterates (θ_k, ψ_k) obtained by simultaneous gradient descent is monotonically increasing.

Proof. The first part is a direct consequence of Lemma A.4 and Lemma 2.2.

To see the the norms of the iterates (θ_k, ψ_k) is monotonically increasing, we calculate

$$\begin{aligned} & \theta_{k+1}^2 + \psi_{k+1}^2 \\ &= (\theta_k - hf'(\theta_k \psi_k) \psi_k)^2 + (\psi_k + hf'(\theta_k \psi_k) \theta_k)^2 \\ &= \theta_k^2 + \psi_k^2 + h^2 f'(\theta_k \psi_k)^2 (\theta_k^2 + \psi_k^2) \\ &\geq \theta_k^2 + \psi_k^2. \end{aligned} \quad (56)$$

□

Lemma 2.5. For alternating gradient descent with n_g generator and n_d discriminator updates, the Jacobian of the update operator $F_h(\theta, \psi)$ has eigenvalues

$$\lambda_{1/2} = 1 - \frac{\alpha^2}{2} \pm \sqrt{\left(1 - \frac{\alpha^2}{2}\right)^2 - 1}. \quad (5)$$

with $\alpha := \sqrt{n_g n_d} h f'(0)$. For $\alpha \leq 2$, all eigenvalues are hence on the unit circle. Moreover for $\alpha > 2$, there are eigenvalues outside the unit circle.

Proof. The update operators for alternating gradient descent are given by

$$F_1(\theta, \psi) = \begin{pmatrix} \theta - hf'(\theta \psi) \psi \\ \psi \end{pmatrix} \quad (57)$$

$$F_2(\theta, \psi) = \begin{pmatrix} \theta \\ \psi + hf'(\theta \psi) \theta \end{pmatrix}. \quad (58)$$

Hence, the Jacobians of these operators at 0 are given by

$$F'_1(0, 0) = \begin{pmatrix} 1 & -hf'(0) \\ 0 & 1 \end{pmatrix} \quad (59)$$

$$F'_2(0, 0) = \begin{pmatrix} 1 & 0 \\ hf'(0) & 1 \end{pmatrix}. \quad (60)$$

As a result, the Jacobian of the combined update operator is

$$\begin{aligned} (F_2^{n_d} \circ F_1^{n_g})'(0, 0) &= F'_2(0, 0)^{n_d} \cdot F'_1(0, 0)^{n_g} \\ &= \begin{pmatrix} 1 & -n_g h f'(0) \\ n_d h f'(0) & -n_g n_d h^2 f'(0)^2 + 1 \end{pmatrix}. \end{aligned} \quad (61)$$

An easy calculation shows that the eigenvalues of this matrix are

$$\lambda_{1/2} = 1 - \frac{\alpha^2}{2} \pm \sqrt{\left(1 - \frac{\alpha^2}{2}\right)^2 - 1} \quad (62)$$

with $\alpha = \sqrt{n_g n_d} h f'(0)$ which are on the unit circle if and only if $\alpha \leq 2$.

□

Lemma 3.1. A WGAN trained with simultaneous or alternating gradient descent with a fixed number of discriminator updates per generator update and a fixed learning rate $h > 0$ does generally not converge to the Nash equilibrium for the Dirac-GAN.

Proof. First, consider simultaneous gradient descent. Assume that the iterates (θ_k, ψ_k) converge towards the equilibrium point $(0, 0)$. Note that $(\theta_{k+1}, \psi_{k+1}) \neq 0$ if $(\theta_k, \psi_k) \neq 0$. We can therefore assume without loss of generality that $(\theta_k, \psi_k) \neq 0$ for all $k \in \mathbb{N}$.

Because $\lim_{k \rightarrow \infty} \psi_k = 0$, there exists k_0 such that for all $k \geq k_0$ we have $|\psi_k| < 1$. For $k \geq k_0$ we therefore have

$$\begin{pmatrix} \theta_{k+1} \\ \psi_{k+1} \end{pmatrix} = \begin{pmatrix} 1 & -h \\ h & 1 \end{pmatrix} \begin{pmatrix} \theta_k \\ \psi_k \end{pmatrix}. \quad (63)$$

For $k \geq k_0$, the iterates are therefore given by

$$\begin{pmatrix} \theta_k \\ \psi_k \end{pmatrix} = A^{k-k_0} \begin{pmatrix} \theta_{k_0} \\ \psi_{k_0} \end{pmatrix} \quad \text{with } A = \begin{pmatrix} 1 & -h \\ h & 1 \end{pmatrix}. \quad (64)$$

However, the eigenvalues of A are given by $\lambda_{1/2} = 1 \pm hi$ which both have absolute value $\sqrt{1+h^2} > 1$. This contradicts the assumption that (θ_k, ψ_k) converges to $(0, 0)$.

A similar argument also hold for alternating gradient descent. In this case, A is given by

$$\begin{pmatrix} 1 & 0 \\ h & 1 \end{pmatrix}^{n_d} \begin{pmatrix} 1 & -h \\ 0 & 1 \end{pmatrix}^{n_g} = \begin{pmatrix} 1 & -hn_g \\ hn_d & 1 - h^2 n_g n_d \end{pmatrix}. \quad (65)$$

The eigenvalues of A as in (65) are given by

$$1 - \frac{h^2 n_g n_h}{2} \pm \sqrt{\left(1 - \frac{h^2 n_g n_h}{2}\right)^2 - 1}. \quad (66)$$

At least one of these eigenvalues has absolute value greater or equal to 1. Note that for almost all initial conditions (θ_0, ψ_0) , the the inner product between the eigenvector corresponding to the eigenvalue with modulus bigger than 1 will be nonzero for all $k \in \mathbb{N}$. Since the recursion in (63) is linear, this contradicts the fact that $(\theta_k, \psi_k) \rightarrow (0, 0)$, showing that alternating gradient descent generally does not converge to the Nash-equilibrium either. □

Lemma 3.2. When using Gaussian instance noise with standard deviation σ , the eigenvalues of the Jacobian of the gradient vector field are given by

$$\lambda_{1/2} = f''(0)\sigma^2 \pm \sqrt{f''(0)^2\sigma^4 - f'(0)^2}. \quad (6)$$

In particular, all eigenvalues of the Jacobian have negative real-part at the Nash-equilibrium if $f''(0) < 0$ and $\sigma > 0$. Hence, simultaneous and alternating gradient descent are both locally convergent for small enough learning rates.

Proof. When using instance noise, the GAN training objective (1) is given by

$$\mathbb{E}_{\tilde{\theta} \sim \mathcal{N}(\theta, \sigma^2)} [f(\tilde{\theta}\psi)] + \mathbb{E}_{x \sim \mathcal{N}(0, \sigma^2)} [f(-x\psi)]. \quad (67)$$

The corresponding gradient vector field is hence given by

$$\tilde{v}(\theta, \psi) = \mathbb{E}_{\tilde{\theta}, x} \begin{pmatrix} -\psi f'(\tilde{\theta}\psi) \\ \tilde{\theta} f'(\tilde{\theta}\psi) - x f'(-x\psi) \end{pmatrix}. \quad (68)$$

The Jacobian $\tilde{v}'(\theta, \psi)$ is therefore

$$\mathbb{E}_{\tilde{\theta}, x} \begin{pmatrix} -f''(\tilde{\theta}\psi)\psi^2 & -f'(\tilde{\theta}\psi) - f''(\tilde{\theta}\psi)\tilde{\theta}\psi \\ f'(\tilde{\theta}\psi) + f''(\tilde{\theta}\psi)\tilde{\theta}\psi & f''(\tilde{\theta}\psi)\tilde{\theta}^2 + x^2 f(-x\psi) \end{pmatrix} \quad (69)$$

Evaluating it at $\theta = \psi = 0$ yields

$$\tilde{v}'(0, 0) = \begin{pmatrix} 0 & -f'(0) \\ f'(0) & 2f''(0)\sigma^2 \end{pmatrix} \quad (70)$$

whose eigenvalues are given by

$$\lambda_{1/2} = f''(0)\sigma^2 \pm \sqrt{f''(0)^2\sigma^4 - f'(0)^2}. \quad (71)$$

□

Lemma 3.3. *The eigenvalues of the Jacobian of the gradient vector field for the gradient-regularized Dirac-GAN at the equilibrium point are given by*

$$\lambda_{1/2} = -\frac{\gamma}{2} \pm \sqrt{\frac{\gamma^2}{4} - f'(0)^2}. \quad (8)$$

In particular, for $\gamma > 0$ all eigenvalues have negative real part. Hence, simultaneous and alternating gradient descent are both locally convergent for small enough learning rates.

Proof. The regularized gradient vector field becomes

$$\tilde{v}(\theta, \psi) = \begin{pmatrix} -f'(\theta\psi)\psi \\ f'(\theta\psi)\theta - \gamma\psi \end{pmatrix}. \quad (72)$$

The Jacobian $\tilde{v}'(\theta, \psi)$ is therefore given by

$$\begin{pmatrix} -f''(\theta\psi)\psi^2 & -f'(\theta\psi) - f''(\theta\psi)\theta\psi \\ f'(\theta\psi) + f''(\theta\psi)\theta\psi & f''(\theta\psi)\theta^2 - \gamma \end{pmatrix}. \quad (73)$$

Evaluating it at $\theta = \psi = 0$ yields

$$\tilde{v}'(0, 0) = \begin{pmatrix} 0 & -f'(0) \\ f'(0) & -\gamma \end{pmatrix} \quad (74)$$

whose eigenvalues are given by

$$\lambda_{1/2} = -\frac{\gamma}{2} \pm \sqrt{\frac{\gamma^2}{4} - f'(0)^2}. \quad (75)$$

□

C. Other regularization strategies

In this section we discuss further regularization techniques for GANs on our example problem that were omitted in the main text due to space constraints.

C.1. Nonsaturating GAN

Especially in the beginning of training, the discriminator can reject samples produced by the generator with high confidence (Goodfellow et al., 2014). When this happens, the loss for the generator may saturate so that the generator receives almost no gradient information anymore.

To circumvent this problem Goodfellow et al. (2014) introduced a nonsaturating objective for the generator. In nonsaturating GANs, the generator objective is replaced with⁷

$$\max_{\theta} \mathbb{E}_{p_{\theta}(x)} f(-D_{\psi}(x)). \quad (76)$$

In our example, this is $\max_{\theta} f(-\psi\theta)$.

While the nonsaturating generator objective was originally motivated by global stability considerations, we investigate its effect on local convergence. A linear analysis similar to normal GANs yields

Lemma C.1. *The unique Nash-equilibrium for the nonsaturating GAN on the example problem is given by $\theta = \psi = 0$. The eigenvalues of the Jacobian of the gradient vector field at the equilibrium are $\pm f'(0)i$ which are both on the imaginary axis.*

Proof. The gradient vector field for the nonsaturating GAN is given by

$$v(\theta, \psi) = \begin{pmatrix} -f'(-\theta\psi)\psi \\ f'(\theta\psi)\theta \end{pmatrix}. \quad (77)$$

As in the proof of Lemma 2.2, we see that $(\psi, \theta) = (0, 0)$ defines the unique Nash-equilibrium for the nonsaturating GAN.

Moreover, the Jacobian $v'(\theta, \psi)$ is

$$\begin{pmatrix} f''(-\theta\psi)\psi^2 & -f'(-\theta\psi) + f''(-\theta\psi)\theta\psi \\ f'(\theta\psi) + f''(\theta\psi)\theta\psi & f''(\theta\psi)\theta^2 \end{pmatrix}. \quad (78)$$

At $\theta = \psi = 0$ we therefore have

$$v'(0, 0) = \begin{pmatrix} 0 & -f'(0) \\ f'(0) & 0 \end{pmatrix}. \quad (79)$$

with eigenvalues $\lambda_{1/2} = \pm f'(0)i$. □

Lemma C.1 implies that simultaneous gradient descent is not locally convergent for a nonsaturating GAN and any

⁷Goodfellow et al. (2014) used $f(t) = -\log(1 + \exp(-t))$.

learning rate $h > 0$, because the eigenvalues of the Jacobian of the corresponding update operator F_h all have absolute value larger than 1 (Lemma A.4). While Lemma C.1 also rules out linear convergence towards the Nash-equilibrium in the continuous case (i.e. for $h \rightarrow 0$), the continuous training dynamics could in principle still converge with a sublinear convergence rate. Indeed, we find this to be the case for the Dirac-GAN. We have

Lemma C.2. *For every integral curve of the gradient vector field of the nonsaturating Dirac-GAN we have*

$$\frac{d}{dt}(\theta(t)^2 + \psi(t)^2) = 2[f'(\theta\psi) - f'(-\theta\psi)]\theta\psi. \quad (80)$$

For concave f this is nonpositive. Moreover, for $f''(0) < 0$, the continuous training dynamics of the nonsaturating Dirac-GAN converge with logarithmic convergence rate.

Proof. The gradient vector field for the nonsaturating Dirac-GAN is given by

$$v(\theta, \psi) = \begin{pmatrix} -f'(-\theta\psi)\psi \\ f'(\theta\psi)\theta \end{pmatrix}. \quad (81)$$

Hence, we have

$$\begin{aligned} \frac{d}{dt}(\theta(t)^2 + \psi(t)^2) &= v_1(\theta, \psi)\theta + v_2(\theta, \psi)\psi \\ &= 2\theta\psi[f'(\theta\psi) - f'(-\theta\psi)]. \end{aligned} \quad (82)$$

For concave f , we have

$$\frac{f'(\theta\psi) - f'(-\theta\psi)}{2\theta\psi} \leq 0 \quad (83)$$

and hence

$$\frac{d}{dt}(\theta(t)^2 + \psi(t)^2) \leq 0. \quad (84)$$

Now assume that $f'(0) \neq 0$ and $f''(0) < 0$.

To intuitively understand why the continuous system converges with logarithmic convergence rate, note that near the equilibrium point we asymptotically have in polar coordinates $(\theta, \psi) = (\sqrt{w} \cos(\phi), \sqrt{w} \sin(\phi))$:

$$\dot{\phi} = f'(0) + \mathcal{O}(|w|^{1/2}) \quad (85)$$

$$\dot{w} = 4f''(0)\theta^2\psi^2 + \mathcal{O}(|\theta\psi|^4) \quad (86)$$

$$= f''(0)w^2 \sin^2(2\phi) + \mathcal{O}(|w|^4). \quad (87)$$

When we ignore higher order terms, we can solve this sys-

tem analytically⁸ for ϕ and w :

$$\phi(t) = f'(0)(t - t_0) \quad (89)$$

$$w(t) = \frac{2}{-f''(0)t + \frac{f''(0)}{4f'(0)} \sin(4f'(0)(t - t_0)) + c} \quad (90)$$

The training dynamics are hence convergent with logarithmic convergence rate $\mathcal{O}\left(\frac{1}{\sqrt{t}}\right)$.

For a more formal proof, first note that w is nonincreasing by the first part of the proof. Moreover, for every $\epsilon > 0$ there is $\delta > 0$ such that for $w < \delta$:

$$f'(0) - \epsilon \leq \dot{\phi} \leq f'(0) + \epsilon \quad (91)$$

$$\dot{w} \leq (f''(0) \sin^2(2\phi) + \epsilon)w^2. \quad (92)$$

This implies that for every time interval $[0, T]$, $\phi(t)$ is in

$$\bigcup_{k \in \mathbb{Z}} \left[\frac{\pi}{8} + k \frac{\pi}{2}, \frac{3\pi}{8} + k \frac{\pi}{2} \right] \quad (93)$$

for t in a union of intervals $Q_T \subseteq [0, T]$ with total length at least $\beta \lfloor \alpha T \rfloor$ with some constants $\alpha, \beta > 0$ which are independent of T .

For these $t \in Q_T$ we have $\sin^2(2\phi(t)) \geq \frac{1}{2}$. Because $f''(0) < 0$, this shows

$$\dot{w}(t) \leq \left(\frac{1}{2}f''(0) + \epsilon \right) w(t)^2 \quad (94)$$

for $t \in Q_T$ and ϵ small enough. Solving the right hand formally yields

$$w(t) \leq \frac{1}{-(\frac{1}{2}f''(0) + \epsilon)t + c}. \quad (95)$$

As $w(t)$ is nonincreasing for $t \notin Q_T$ and the total length of Q_T is at least $\beta \lfloor \alpha T \rfloor$ this shows that

$$w(T) \leq \frac{1}{-(\frac{1}{2}f''(0) + \epsilon)\beta \lfloor \alpha T \rfloor + c}. \quad (96)$$

The training dynamics hence converge with logarithmic convergence rate $\mathcal{O}\left(\frac{1}{\sqrt{t}}\right)$. \square

Note that the standard choice $f(t) = -\log(1 + \exp(-t))$ is concave and satisfies $f''(0) = -\frac{1}{4} < 0$. Lemma C.1 is hence applicable and shows that the GAN training dynamics for the standard choice of f converge with logarithmic convergence rate in the continuous case. The training behavior of the nonsaturating GAN on our example problem is visualized in Figure 3b.

⁸For solving the ODE we use the *separation of variables*-technique and the identity

$$\int 2 \sin^2(ax) dx = x - \frac{\sin(2ax)}{2a}. \quad (88)$$

C.2. Wasserstein GAN-GP

In practice, it can be hard to enforce the Lipschitz-constraint for WGANs. A practical solution to this problem was given by Gulrajani et al. (2017), who derived a simple gradient penalty with a similar effect as the Lipschitz-constraint. The resulting training objective is commonly referred to as WGAN-GP.

Similarly to WGANs, we find that WGAN-GP does not converge for the Dirac-GAN. A similar analysis also applies to the DRAGAN-regularizer proposed by Kodali et al. (2017).

The regularizer proposed by Gulrajani et al. (2017) is given by

$$R(\psi) = \frac{\gamma}{2} E_{\hat{x}} (\|\nabla_x D_\psi(\hat{x})\| - g_0)^2 \quad (97)$$

where \hat{x} is sampled uniformly on the line segment between two random points $x_1 \sim p_\theta(x_1)$, $x_2 \sim p_D(x_2)$.

For the Dirac-GAN, it simplifies to

$$R(\psi) = \frac{\gamma}{2} (|\psi| - g_0)^2 \quad (98)$$

The corresponding gradient vector field is given by

$$\tilde{v}(\theta, \psi) = \begin{pmatrix} -\psi \\ \theta - \text{sign}(\psi)\gamma(|\psi| - g_0) \end{pmatrix}. \quad (99)$$

Note that the gradient vector field has a discontinuity at the equilibrium point, as the gradient vector field takes on values with norm bigger than some fixed constant in every neighborhood of the equilibrium point. As a result, we have

Lemma C.3. *WGAN-GP trained with simultaneous or alternating gradient descent with a fixed number of generator and discriminator updates and a fixed learning rate $h > 0$ does not converge locally to the Nash equilibrium for the Dirac-GAN.*

Proof. First, consider simultaneous gradient descent. Assume that the iterates (θ_k, ψ_k) converge towards the equilibrium point $(0, 0)$. For almost all initial conditions⁹ we have $(\theta_k, \psi_k) \neq (0, 0)$ for all $k \in \mathbb{N}$. This implies

$$|\psi_{k+1} - \psi_k| = h|\theta_k - \gamma\psi_k - \text{sign}(\psi_k)g_0| \quad (100)$$

and hence $\lim_{k \rightarrow \infty} |\psi_{k+1} - \psi_k| = h|g_0| \neq 0$, showing that (θ_k, ψ_k) is not a Cauchy sequence. This contradicts the assumption that (θ_k, ψ_k) converges to the equilibrium point $(0, 0)$.

A similar argument also holds for alternating gradient descent. \square

The training behavior of WGAN-GP on our example problem is visualized in Figure 3d.

⁹Depending on γ , h and g_0 modulo a set of measure 0.

As for WGANs, we stress that this analysis only holds if the discriminator is trained with a fixed number of discriminator updates per generator update. Again, more careful training that ensures that the discriminator is kept exactly optimal or two-timescale training (Heusel et al., 2017) might be able to ensure convergence for WGAN-GP.

C.3. Consensus optimization

Consensus optimization (Mescheder et al., 2017) is an algorithm that attempts to solve the problem of eigenvalues with zero real-part by introducing a regularization term that explicitly moves the eigenvalues to the left. The regularization term in consensus optimization is given by

$$\begin{aligned} R(\theta, \psi) &= \frac{\gamma}{2} \|v(\theta, \psi)\|^2 \\ &= \frac{\gamma}{2} (\|\nabla_\theta L(\theta, \psi)\|^2 + \|\nabla_\psi L(\theta, \psi)\|^2). \end{aligned} \quad (101)$$

As was proved by Mescheder et al. (2017), consensus optimization converges locally for small learning rates $h > 0$ provided that the Jacobian $v'(\theta^*, \psi^*)$ is invertible.¹⁰

Indeed, for the Dirac-GAN we have

Lemma C.4. *The eigenvalues of the Jacobian of the gradient vector field for consensus optimization at the equilibrium point are given by*

$$\lambda_{1/2} = -\gamma f'(0)^2 \pm i f'(0) \quad (102)$$

In particular, all eigenvalues have a negative real part $-\gamma f'(0)^2$. Hence, simultaneous and alternating gradient descent are both locally convergent using consensus optimization for small enough learning rates.

Proof. As was shown by Mescheder et al. (2017), the Jacobian of the modified vector field \tilde{v} at the equilibrium point is

$$\tilde{v}'(0, 0) = v'(0, 0) - \gamma v'(0, 0)^\top v'(0, 0). \quad (103)$$

In our case, this is

$$\begin{pmatrix} -\gamma f'(0)^2 & -f'(0) \\ f'(0) & -\gamma f'(0)^2 \end{pmatrix}. \quad (104)$$

A simple calculation shows that the eigenvalues of $\tilde{v}'(0, 0)$ are given by

$$\lambda_{1/2} = -\gamma f'(0)^2 \pm i f'(0). \quad (105)$$

This concludes the proof. \square

¹⁰Mescheder et al. (2017) considered only the case of isolated equilibrium points. However, by applying Theorem A.3, it is straightforward to generalize their proof to the case where we are confronted with a submanifold of equivalent equilibrium points.

A visualization of consensus optimization for the Dirac-GAN is given in Figure 3e.

Unfortunately, consensus optimization has the drawback that it can introduce new spurious points of attraction to the GAN training dynamics. While this is usually not a problem for simple examples, it can be a problem for more complex ones like deep neural networks.

A similar regularization term as in consensus optimization was also independently proposed by [Nagarajan & Kolter \(2017\)](#). However, [Nagarajan & Kolter \(2017\)](#) proposed to only regularize the component $\nabla_\psi L(\theta, \psi)$ of the gradient vector field corresponding to the discriminator parameters. Moreover, the regularization term is only added to the generator objective to give the generator more foresight. It can be shown ([Nagarajan & Kolter, 2017](#)) that this simplified regularization term can in certain situations also make the training dynamics locally convergent, but might be better behaved at stationary points of the GAN training dynamics that do not correspond to a local Nash-equilibrium. Indeed, a more detailed analysis shows that this simplified regularization term behaves similarly to instance noise and gradient penalties (which we discussed in Section 3.2 and Section 3.3) for the Dirac-GAN.

D. General convergence results

In this section, we prove Theorem 4.1. To this end, we extend the convergence proof by [Nagarajan & Kolter \(2017\)](#) to our setting. We show that by introducing the gradient penalty terms $R_i(\theta, \psi)$, we can get rid of the assumption that the generator and data distributions locally have the same support. As we have seen, this makes the theory applicable to more realistic cases, where both the generator and data distributions typically lie on lower dimensional manifolds.

D.1. Convergence proof

To prove Theorem 4.1, we first need to understand the local structure of the gradient vector field $v(\theta, \psi)$. Recall that the gradient vector field $v(\theta, \psi)$ is defined as

$$v(\theta, \psi) := \begin{pmatrix} -\nabla_\theta L(\theta, \psi) \\ \nabla_\psi L(\theta, \psi) \end{pmatrix} \quad (106)$$

with

$$\begin{aligned} L(\theta, \psi) = & \mathbb{E}_{p(z)} [f(D_\psi(G_\theta(z)))] \\ & + \mathbb{E}_{p_D(x)} [f(-D_\psi(x))]. \end{aligned} \quad (107)$$

Lemma D.1. *The gradient of $L(\theta, \psi)$ with respect to θ is given by*

$$\begin{aligned} \nabla_\theta L(\theta, \psi) = & \mathbb{E}_{p(z)} [f'(D_\psi(G_\theta(z))) [\nabla_\theta G_\theta(z)]^\top \\ & \cdot \nabla_x D_\psi(G_\theta(z))]. \end{aligned} \quad (108)$$

Similarly, the gradient of $L(\theta, \psi)$ with respect to ψ is given by

$$\begin{aligned} \nabla_\psi L(\theta, \psi) = & \mathbb{E}_{p_\theta(x)} [f'(D_\psi(x)) \nabla_\psi D_\psi(x)] \\ & - \mathbb{E}_{p_D(x)} [f'(-D_\psi(x)) \nabla_\psi D_\psi(x)]. \end{aligned} \quad (109)$$

Proof. This is just the chain rule. \square

Lemma D.2. *Assume that (θ^*, ψ^*) satisfies Assumption I. The Jacobian of the gradient vector field $v(\theta, \psi)$ at (θ^*, ψ^*) is then*

$$v'(\theta^*, \psi^*) = \begin{pmatrix} 0 & -K_{DG}^\top \\ K_{DG} & K_{DD} \end{pmatrix}. \quad (110)$$

The terms K_{DD} and K_{DG} are given by

$$K_{DD} = 2f''(0) \mathbb{E}_{p_D(x)} [\nabla_\psi D_{\psi^*}(x) \nabla_\psi D_{\psi^*}(x)^\top] \quad (111)$$

$$K_{DG} = f'(0) \nabla_\theta \mathbb{E}_{p_\theta(x)} [\nabla_\psi D_{\psi^*}(x)] |_{\theta=\theta^*} \quad (112)$$

Proof. First note that by the definition of $v(\theta, \psi)$ in (106), the Jacobian $v'(\theta^*, \psi^*)$ of $v(\theta, \psi)$ is given by

$$\begin{pmatrix} -\nabla_\theta^2 L(\theta^*, \psi^*) & -\nabla_{\theta,\psi}^2 L(\theta^*, \psi^*) \\ \nabla_{\theta,\psi}^2 L(\theta^*, \psi^*) & \nabla_\psi^2 L(\theta^*, \psi^*) \end{pmatrix}. \quad (113)$$

By Assumption I, $D_{\psi^*}(x) = 0$ in some neighborhood of $\text{supp } p_D$. Hence, we also have $\nabla_x D_{\psi^*}(x) = 0$ and $\nabla_x^2 D_{\psi^*}(x) = 0$ for $x \in \text{supp } p_D$. By taking the derivative of (108) with respect to θ and using $\nabla_x D_{\psi^*}(x) = 0$ and $\nabla_x^2 D_{\psi^*}(x) = 0$ for $x \in \text{supp } p_D$ we see that $\nabla_\theta^2 L(\theta^*, \psi^*) = 0$.

To show (111) and (112), simply take the derivative of (109) with respect to θ and ψ and evaluate at it at $(\theta, \psi) = (\theta^*, \psi^*)$. \square

We now take a closer look at the regularized vector field. Recall that we consider the two regularization terms

$$R_1(\theta, \psi) := \frac{\gamma}{2} \mathbb{E}_{p_D(x)} [\|\nabla_x D_\psi(x)\|^2] \quad (114)$$

$$R_2(\theta, \psi) := \frac{\gamma}{2} \mathbb{E}_{p_\theta(x)} [\|\nabla_x D_\psi(x)\|^2]. \quad (115)$$

As discussed in Section 4.1, the regularization is only applied to the discriminator. The regularized vector field is hence given by

$$\tilde{v}(\theta, \psi) := \begin{pmatrix} -\nabla_\theta L(\theta, \psi) \\ \nabla_\psi L(\theta, \psi) - \nabla_\psi R_i(\theta, \psi) \end{pmatrix}. \quad (116)$$

Lemma D.3. *The gradient $\nabla_\psi R_i(\theta, \psi)$ of the regularization terms R_i , $i \in \{1, 2\}$, with respect to ψ are*

$$\nabla_\psi R_1(\theta, \psi) = \gamma \mathbb{E}_{p_D(x)} [\nabla_{\psi,x} D_\psi(x) \nabla_x D_\psi(x)] \quad (117)$$

$$\nabla_\psi R_2(\theta, \psi) = \gamma \mathbb{E}_{p_\theta(x)} [\nabla_{\psi,x} D_\psi(x) \nabla_x D_\psi(x)]. \quad (118)$$

Proof. These equations can be derived by taking the derivative of (114) and (115) with respect to ψ . \square

Lemma D.4. *The second derivatives $\nabla_\psi^2 R_i(\theta^*, \psi^*)$ of the regularization terms R_i , $i \in \{1, 2\}$, with respect to ψ at (θ^*, ψ^*) are both given by*

$$L_{DD} := \gamma \mathbb{E}_{p_D(x)} [\nabla_{\psi,x} D_{\psi^*}(x) \nabla_{\psi,x} D_{\psi^*}(x)^T]. \quad (119)$$

Moreover, both regularization terms satisfy $\nabla_{\theta,\psi} R_i(\theta^*, \psi^*) = 0$.

Proof. $\nabla_\psi^2 R_i(\theta^*, \psi^*)$, $i \in \{1, 2\}$, can be computed by taking the derivative of (117) and (118) with respect to ψ and using the fact that $\nabla_x D_{\psi^*}(x) = 0$ in a neighborhood of $\text{supp } p_D$.

Moreover, we clearly have $\nabla_{\theta,\psi} R_1(\theta^*, \psi^*) = 0$, because R_1 does not depend on θ . To see that $\nabla_{\theta,\psi} R_2(\theta^*, \psi^*) = 0$, take the derivative of (118) with respect to θ and use the fact that $\nabla_x D_{\psi^*}(x) = 0$ and $\nabla_x^2 D_{\psi^*}(x) = 0$ for $x \in \text{supp } p_D$. \square

As a result, the Jacobian $\tilde{v}'(\theta^*, \psi^*)$ of the regularized gradient vector field at the equilibrium point is given by

$$\tilde{v}'(\theta^*, \psi^*) = \begin{pmatrix} 0 & -K_{DG}^T \\ K_{DG} & K_{DD} - L_{DD} \end{pmatrix}. \quad (120)$$

For brevity, we define $M_{DD} := K_{DD} - L_{DD}$.

To prove Theorem 4.1, we have to show that $\tilde{v}'(\theta^*, \psi^*)$ is well behaved when restricting it to the space orthogonal to the tangent space of $\mathcal{M}_G \times \mathcal{M}_D$ at (θ^*, ψ^*) :

Lemma D.5. *Assume that Assumptions II and III hold. If $v \neq 0$ is not in the tangent space of \mathcal{M}_D at ψ^* , then $\bar{v}^T M_{DD} v < 0$.*

Proof. By Lemma D.2, we have

$$v^T K_{DD} v = 2f''(0) \mathbb{E}_{p_D(x)} [(\nabla_\psi D_{\psi^*}(x)^T v)^2] \quad (121)$$

and by Lemma D.4

$$v^T L_{DD} v = \gamma \mathbb{E}_{p_D(x)} [\|\nabla_{x,\psi} D_{\psi^*}(x)v\|^2]. \quad (122)$$

By Assumption II, we have $f''(0) < 0$. Hence, $v^T M_{DD} v \leq 0$ and $v^T M_{DD} v = 0$ implies

$$\nabla_\psi D_{\psi^*}(x)^T v = 0 \quad \text{and} \quad \nabla_{x,\psi} D_{\psi^*}(x)v = 0 \quad (123)$$

for all $x \in \text{supp } p_D$.

Let

$$h(\psi) := \mathbb{E}_{p_D(x)} [|D_\psi(x)|^2 + \|\nabla_x D_\psi(x)\|^2]. \quad (124)$$

Using the fact that $D_\psi(x) = 0$ and $\nabla_x D_\psi(x) = 0$ for $x \in \text{supp } p_D$, we see that the Hessian of $h(\psi)$ at ψ^* is

$$\nabla_\psi^2 h(\psi^*) = 2 \mathbb{E}_{p_D(x)} [\nabla_\psi D_\psi(x) \nabla_\psi D_\psi(x)^T + \nabla_{\psi,x} D_\psi(x) \nabla_{\psi,x} D_\psi(x)^T] \quad (125)$$

The second directional derivate $\partial_v^2 h(\psi)$ is therefore

$$\partial_v^2 h(\psi) = 2 \mathbb{E}_{p_D(x)} [|\nabla_\psi D_\psi(x)^T v|^2 + \|\nabla_{x,\psi} D_\psi(x)v\|^2] = 0. \quad (126)$$

By Assumption III, this can only hold if v is in the tangent space of \mathcal{M}_D at ψ^* . \square

Lemma D.6. *Assume that Assumption III holds. If $w \neq 0$ is not in the tangent space of \mathcal{M}_G at θ^* , then $K_{DG} w \neq 0$.*

Proof. By Lemma D.2, we have

$$K_{DG} w = f'(0) [\nabla_\theta \mathbb{E}_{p_\theta(x)} [\nabla_\psi D_{\psi^*}(x)] |_{\theta=\theta^*}] w = f'(0) \partial_w g(\theta). \quad (127)$$

for

$$g(\theta) := \mathbb{E}_{p_\theta(x)} [\nabla_\psi D_{\psi^*}(x)]. \quad (128)$$

By Assumption III, this implies $K_{DG} w \neq 0$ if w is not in the tangent space of \mathcal{M}_G at θ^* . \square

We are now ready to prove Theorem 4.1:

Theorem 4.1. *Assume Assumption I, II and III hold for (θ^*, ψ^*) . For small enough learning rates, simultaneous and alternating gradient descent for \tilde{v}_1 and \tilde{v}_2 are both convergent to $\mathcal{M}_G \times \mathcal{M}_D$ in a neighborhood of (θ^*, ψ^*) . Moreover, the rate of convergence is at least linear.*

Proof. First note that by Lemma D.1 and Lemma D.3 $v(\theta, \psi) = 0$ for all points $(\theta, \psi) \in \mathcal{M}_G \times \mathcal{M}_D$, because $D_\psi(x) = 0$ and $\nabla_x D_\psi(x) = 0$ for all $x \in \text{supp } p_D$ and $\psi \in \mathcal{M}_D$. Hence, $\mathcal{M}_G \times \mathcal{M}_D$ consists only of equilibrium points of the regularized gradient vector fields.

Let $\mathcal{T}_{\theta^*} \mathcal{M}_G$ and $\mathcal{T}_{\psi^*} \mathcal{M}_D$ denote the tangent spaces of \mathcal{M}_G and \mathcal{M}_D at θ^* and ψ^* .

We now want to show that both simultaneous and alternating gradient descent are locally convergent to $\mathcal{M}_G \times \mathcal{M}_D$ for the regularized gradient vector field $\tilde{v}(\theta, \psi)$. To this end, we want to apply Theorem A.3. By choosing local coordinates $\theta(\alpha, \gamma_G)$ and $\psi(\beta, \gamma_D)$ for \mathcal{M}_G and \mathcal{M}_D and using Remark A.6, we can assume without loss of generality that $\theta^* = 0, \psi^* = 0$ as well as

$$\mathcal{M}_G = \mathcal{T}_{\theta^*} \mathcal{M}_G = \{0\}^k \times \mathbb{R}^{n-k} \quad (129)$$

$$\mathcal{M}_D = \mathcal{T}_{\psi^*} \mathcal{M}_D = \{0\}^l \times \mathbb{R}^{m-l}. \quad (130)$$

This allows us to write¹¹ $\tilde{v}(\theta, \psi) = \tilde{v}(\alpha, \gamma_G, \beta, \gamma_D)$. In order to apply Theorem A.3, we have to show that $\nabla_{(\alpha, \beta)}\tilde{v}(\theta^*, \psi^*)$ only has eigenvalues with negative real-part.

By Lemma D.2, $\nabla_{(\alpha, \beta)}\tilde{v}(\theta^*, \psi^*)$ is of the form

$$\begin{pmatrix} 0 & -\tilde{K}_{DG}^\top \\ \tilde{K}_{DG} & \tilde{K}_{DD} - \tilde{L}_{DD} \end{pmatrix} \quad (131)$$

where \tilde{K}_{DD} , \tilde{K}_{DG} and \tilde{L}_{DD} denote the submatrices of K_{DD} , K_{DG} and L_{DD} corresponding to the (α, β) coordinates.

We now show that $\tilde{M}_{DD} := \tilde{K}_{DD} - \tilde{L}_{DD}$ is negative definite and \tilde{K}_{DG} has full column rank.

To this end, first note that

$$\tilde{v}^\top \tilde{M}_{DD} \tilde{v} = v^\top M_{DD} v \quad (132)$$

with $v^\top := (\tilde{v}^\top, 0)$. Note that $v \notin \mathcal{T}_{\psi^*}\mathcal{M}_D$ for $\tilde{v} \neq 0$. Hence, by Lemma D.5 we have that $\tilde{v}^\top \tilde{M}_{DD} \tilde{v} < 0$ if $\tilde{v} \neq 0$. As a result, we see that \tilde{M}_{DD} is symmetric negative definite.

Similarly, for $w^\top := (\tilde{w}^\top, 0)$, the components of $K_{DG}w$ corresponding to the β -coordinates are given by $\tilde{K}_{DG}\tilde{w}$. Again, we have $w \notin \mathcal{T}_{\theta^*}\mathcal{M}_G$ for $\tilde{w} \neq 0$. Hence, by Lemma D.6 we have that $K_{DG}w \neq 0$ if $\tilde{w} \neq 0$. Because the components of $K_{DG}w$ corresponding to the γ_D coordinates are 0, this shows that $\tilde{K}_{DG}\tilde{w} \neq 0$. \tilde{K}_{DG} therefore has full column rank.

Theorem A.7 now implies that all eigenvalues of $\nabla_{(\alpha, \beta)}\tilde{v}(\theta^*, \psi^*)$ have negative real part. By Lemma A.4, Lemma A.5 and Theorem A.3, simultaneous and alternating gradient descent are therefore both convergent to $\mathcal{M}_G \times \mathcal{M}_D$ near (θ^*, ψ^*) for small enough learning rates. Moreover, the rate of convergence is at least linear. \square

D.2. Extensions

In the proof of Theorem 4.1 we have assumed that $f''(0) < 0$. This excludes the function $f(t) = t$ which is used in Wasserstein-GANs. We now show that our convergence proof extends to the case where $f(t) = t$ when we modify Assumption III as little bit:

Remark D.7. When we replace $h(\psi)$ with

$$\tilde{h}(\psi) := \mathbb{E}_{p_D(x)} [\|\nabla_x D_\psi(x)\|^2] \quad (133)$$

and \mathcal{M}_D with $\tilde{\mathcal{M}}_D := \{\psi \mid \tilde{h}(\psi) = 0\}$ the results of Theorem 4.1 still hold for $f(t) = t$.

Proof. Almost everything in the proof of Theorem 4.1 still holds for these modified assumptions. The only thing that

¹¹By abuse of notation, we simply write $\theta = (\alpha, \gamma_G)$ and $\psi = (\beta, \gamma_D)$.

we have to show is that $\mathcal{M}_G \times \mathcal{M}_D$ still consists only of equilibrium points and that Lemma D.5 still holds in this setting.

To see the former, note that by Lemma D.1 we still have $\nabla_\theta L(\theta, \psi) = 0$ for $(\theta, \psi) \in \mathcal{M}_G \times \mathcal{M}_D$, because we have $\nabla_x D_\psi(x) = 0$ for $\psi \in \mathcal{M}_D$ and $x \in \text{supp } p_D$. On the other hand, for $f(t) = t$ we also have $\nabla_\psi L(\theta, \psi) = 0$ if $\theta \in \mathcal{M}_G$, because for $\theta \in \mathcal{M}_G$ the definition of \mathcal{M}_G implies that $p_\theta = p_D$ and hence, by Lemma D.1,

$$\begin{aligned} \nabla_\psi L(\theta, \psi) &= \mathbb{E}_{x \sim p_D} [\nabla_\psi D_\psi(x)] \\ &\quad - \mathbb{E}_{x \sim p_D} [\nabla_\psi D_\psi(x)] = 0. \end{aligned} \quad (134)$$

To see why Lemma D.5 still holds, first note that for $f(t) = t$, we have $f''(0) = 0$, so that by Lemma D.2 $K_{DD} = 0$. Hence,

$$v^\top M_{DD} v = -v^\top L_{DD} v. \quad (135)$$

We therefore have to show that $v^\top L_{DD} v \neq 0$ if v is not in the tangent space of \mathcal{M}_D .

However, we have seen in the proof of Lemma D.5 that

$$v^\top L_{DD} v = \gamma \mathbb{E}_{p_D(x)} [\|\nabla_{x, \psi} D_{\psi^*}(x)v\|^2]. \quad (136)$$

Hence $v^\top L_{DD} v = 0$ implies $\nabla_{x, \psi} D_{\psi^*}(x)v = 0$ for $x \in \text{supp } p_D$ and thus

$$\partial_v^2 h(\psi) = 2 \mathbb{E}_{p_D(x)} [\|\nabla_{x, \psi} D_\psi(x)v\|^2] = 0. \quad (137)$$

By Assumption III, this can only be the case if v is in the tangent space of \mathcal{M}_D . This concludes the proof. \square

In Section D.1, we showed that both regularizers R_1 and R_2 from Section 4.1 make the GAN training dynamics locally convergent. A similar, but slightly more complex regularizer was also proposed by Roth et al. (2017) who tried to find a computationally efficient approximation to instance noise. The regularizer proposed by Roth et al. (2017) is given by a linear combination of R_1 and R_2 where the weighting is adaptively chosen depending on the logits of $D_\psi(x)$ of the current discriminator at a data point x :

$$\begin{aligned} R_{\text{Roth}}(\theta, \psi) &= \mathbb{E}_{p_\theta(x)} [(1 - \sigma(D_\psi(x)))^2 \|\nabla_x D_\psi(x)\|^2] \\ &\quad + \mathbb{E}_{p_D(x)} [\sigma(D_\psi(x)))^2 \|\nabla_x D_\psi(x)\|^2] \end{aligned} \quad (138)$$

Indeed, we can show that our convergence proof extends to this regularizer (and a slightly more general class of regularizers):

Remark D.8. When we replace the regularization terms R_1 and R_2 with

$$\begin{aligned} R_3(\theta, \psi) &= \mathbb{E}_{p_\theta(x)} [w_1(D_\psi(x)) \|\nabla_x D_\psi(x)\|^2] \\ &\quad + \mathbb{E}_{p_D(x)} [w_2(D_\psi(x)) \|\nabla_x D_\psi(x)\|^2] \end{aligned} \quad (139)$$

so that $w_1(0) > 0$ and $w_2(0) > 0$, the results of Theorem 4.1 still hold.

Proof. Again, we have to show that $\mathcal{M}_G \times \mathcal{M}_D$ still consists only of equilibrium points and that Lemma D.5 still holds in this setting.

However, by using $\nabla_x D_\psi(x) = 0$ for $x \in \text{supp } p_D$ and $\psi \in \mathcal{M}_D$, it is easy to see that $\nabla_\psi R_3(\theta, \psi) = 0$ for all $(\theta, \psi) \in \mathcal{M}_G \times \mathcal{M}_D$, which implies that $\mathcal{M}_G \times \mathcal{M}_D$ still consists only of equilibrium points.

To see why Lemma D.5 still holds in this setting, note that (after a little bit of algebra) we still have $\nabla_{\theta, \psi} R_3(\theta^*, \psi^*) = 0$ and

$$\nabla_\psi^2 R_3(\theta^*, \psi^*) = \frac{1}{\gamma} (w_1(0) + w_2(0)) L_{DD}. \quad (140)$$

The proof of Lemma D.5 therefore still applies in this setting. \square

E. Stable equilibria for unregularized GAN training

In Section 2, we have seen that unregularized GAN training is not always locally convergent to the equilibrium point. Moreover, in Section 4, we have shown that zero-centered gradient penalties make general GANs locally convergent under some suitable assumptions.

While our results demonstrate that we cannot expect unregularized GAN training to lead to local convergence for general GAN architectures, there can be situations where unregularized GAN training has stable equilibria. Such equilibria usually require additional assumptions on the class of representable discriminators.

In this section, we identify two types of stable equilibria. For the first class of stable equilibria, which we call *energy solutions*, the equilibrium discriminator forms an energy function for the true data distributions and might be a partial explanation for the success of autoencoder-based discriminators (Zhao et al., 2016; Berthelot et al., 2017). For the second class, which we call *full-rank solutions*, the discriminator learns a representation of the data distribution with certain properties and might be a partial explanation for the success of batch-normalization for training GANs (Radford et al., 2015).

E.1. Energy Solutions

For technical reasons, we assume that $\text{supp } p_D$ defines a \mathcal{C}^1 -manifold in this section.

Energy solutions are solutions where the discriminator forms a potential function for the true data distribution. Such solutions (θ^*, ψ^*) satisfy the following property:

Assumption I'. We have $p_{\theta^*} = p_D$, $D_{\psi^*}(x) = 0$, $\nabla_x D_{\psi^*}(x) = 0$ and $v^\top \nabla_x^2 D_{\psi^*}(x)v > 0$ for all $x \in \text{supp } p_D$ and v not in the tangent space of $\text{supp } p_D$ at x .

We also need a modified version of Assumption III which ensures certain regularity properties of the reparameterization manifolds \mathcal{M}_G and \mathcal{M}_D near the equilibrium (θ^*, ψ^*) . To formulate Assumption III', we need

$$\tilde{g}(\psi) := \nabla_\theta \mathbb{E}_{p_\theta(x)} [D_\psi(x)]|_{\theta=\theta^*}. \quad (141)$$

Assumption III'. There are ϵ -balls $B_\epsilon(\theta^*)$ and $B_\epsilon(\psi^*)$ around θ^* and ψ^* so that $\mathcal{M}_G \cap B_\epsilon(\theta^*)$ and $\mathcal{M}_D \cap B_\epsilon(\psi^*)$ define \mathcal{C}^1 -manifolds. Moreover, the following holds:

- (i) if v is not in the tangent space of \mathcal{M}_D at ψ^* , then $\partial_v \tilde{g}(\psi^*) \neq 0$.
- (ii) if w is not in the tangent space of \mathcal{M}_G at θ^* , then there is a latent code $z \in \mathbb{R}^k$ so that $\nabla_\theta G_{\theta^*}(z)w$ is not in the tangent space of $\text{supp } p_D$ at $G_{\theta^*}(z) \in \text{supp } p_D$.

The first part of Assumption III' implies that the generator gradients become nonzero whenever the discriminator moves away from an equilibrium discriminator. The second part of Assumption III' means that every time the generator leaves the equilibrium, it pushes some data point away from $\text{supp } p_D$, i.e. the generator is not simply redistributing mass on $\text{supp } p_D$.

In Theorem E.2 we show that energy solutions lead to local convergence of the unregularized GAN training dynamics. For the proof, we first need a generalization of Lemma D.2:

Lemma E.1. Assume that (θ^*, ψ^*) satisfies Assumption I'. The Jacobian of the gradient vector field $v(\theta, \psi)$ at (θ^*, ψ^*) is then given by

$$v'(\theta^*, \psi^*) = \begin{pmatrix} K_{GG} & -K_{DG}^\top \\ K_{DG} & K_{DD} \end{pmatrix}. \quad (142)$$

The terms K_{DD} and K_{DG} are given by

$$K_{GG} = -f'(0) \mathbb{E}_{p(z)} [[\nabla_\theta G_{\theta^*}(z)]^\top \nabla_x^2 D_{\psi^*}(G_{\theta^*}(z)) \nabla_\theta G_{\theta^*}(z)] \quad (143)$$

$$K_{DD} = 2f''(0) \mathbb{E}_{p_D(x)} [\nabla_\psi D_{\psi^*}(x) \nabla_\psi D_{\psi^*}(x)^\top] \quad (144)$$

$$K_{DG} = f'(0) [\nabla_\theta \mathbb{E}_{p_\theta(x)} [\nabla_\psi D_{\psi^*}(x)]|_{\theta=\theta^*}]^\top \quad (145)$$

Proof. Almost all parts of the proof of Lemma D.2 are still valid. The only thing that remains to show is that $\nabla_\theta^2 L(\theta^*, \psi^*) = -K_{GG}$. To see this, just take the derivative of (108) with respect to θ and use the fact that $\nabla_x D_\psi(x) = 0$ for $x \in \text{supp } p_D$. \square

We are now ready to formulate our convergence result for energy solutions:

Theorem E.2. Assume Assumption I', II and III' hold for (θ^*, ψ^*) . Moreover, assume that $f'(0) > 0$. For small enough learning rates, simultaneous and alternating gradient descent for the (unregularized) gradient vector field v are both convergent to $\mathcal{M}_G \times \mathcal{M}_D$ in a neighborhood of (θ^*, ψ^*) . Moreover, the rate of convergence is at least linear.

Proof (Sketch). The proof is similar to the proof of Theorem 4.1.

First, note that $\mathcal{M}_G \times \mathcal{M}_D$ still only consists of equilibrium points. Next, we introduce local coordinates and show that for v not in the tangent space of \mathcal{M}_G at θ^* , we have $v^\top K_{GG} v < 0$. This can be shown using Lemma E.1, Assumption I' and the second part of Assumption III'.

Moreover, we need to show that for w not in the tangent space of \mathcal{M}_D at ψ^* , we have $K_{DG}^\top w \neq 0$. This can be shown by applying the first part of Assumption III'.

The rest of the proof is the same as the proof of Theorem 4.1, except that we have to apply Theorem A.8 instead of Theorem A.7. \square

Note that energy solutions are only possible, if the discriminator is able to satisfy Assumption I'. This is not the case for the Dirac-GAN from Section 2. However, if we use a quadratic discriminator instead, there are also energy solutions to the unregularized GAN training dynamics for the Dirac-GAN. To see this, we can parameterize $D_\psi(x)$ as

$$D_\psi(x) := \psi_1 x^2 + \psi_2 x. \quad (146)$$

It is easy to check that the Dirac-GAN with a discriminator as in (146) indeed has energy solutions: every (θ, ψ) with $\theta = 0$ and $\psi_2 = 0$ defines an equilibrium point of the Dirac-GAN and the GAN-training dynamics are locally convergent near this point if $\psi_1 > 0$. Note however, that even though all equilibria with $\psi_1 > 0$ are points of attraction for the *continuous* GAN training dynamics, they may not be attractors for the *discretized system* when ψ_1 is large and the learning rate h is fixed. In general, the conditioning of energy solutions depends on the condition numbers of the Hessians $\nabla_x^2 D_{\psi^*}(x)$ at all $x \in \text{supp } p_D$. Indeed, the presence of ill-conditioned energy solutions might be one possible explanation why WGAN-GP often works well in practice although it is not even locally convergent for the Dirac-GAN.

E.2. Full-Rank Solutions

In practice, $D_\psi(x)$ is usually implemented by a deep neural network. Such discriminators can be described by functions of the form

$$D_\psi(x) = \psi_1^\top \eta_{\psi_2}(x) \quad (147)$$

with a vector-valued \mathcal{C}^1 -functions η_{ψ_2} and $\psi = (\psi_1, \psi_2)$. η_{ψ_2} can be regarded as a feature-representation of the data point x .

We now state several assumptions that lead to local convergence in this situation.

The first assumption can be seen as a variant of Assumption I adapted to this specific situation:

Assumption I''. We have $p_{\theta^*} = p_D$ and $\psi_1^* = 0$.

We again consider *reparameterization manifolds*, which we define as follows in this section:

$$\mathcal{M}_G := \{\theta \mid p_\theta = p_D\} \quad \mathcal{M}'_D := \{\psi \mid \psi_1 = 0\}. \quad (148)$$

Moreover, let

$$g(\theta) = \mathbb{E}_{p_\theta(x)} [\eta_{\psi_2^*}(x)]. \quad (149)$$

Assumption III now becomes:

Assumption III''. There is an ϵ -ball $B_\epsilon(\theta^*)$ around θ^* so that \mathcal{M}_G defines a \mathcal{C}^1 -manifold¹². Moreover, the following holds:

- (i) The matrix $\mathbb{E}_{p_D(x)} [\eta_{\psi_2^*}(x) \eta_{\psi_2^*}(x)^\top]$ has full rank.
- (ii) if w is not in the tangent space of \mathcal{M}_G at θ^* , then $\partial_w g(\theta^*) \neq 0$.

We call a function $\eta_{\psi_2^*}$ that satisfies the first part of Assumption III'' a *full-rank representation* of p_D . Moreover, if $\eta_{\psi_2^*}$ satisfies the second part of Assumption III'', we call $\eta_{\psi_2^*}$ a *complete representation*, because the second part of Assumption III'' implies that every deviation from the Nash-equilibrium $p_{\theta^*} = p_D$ is detectable using $\eta_{\psi_2^*}$.

In practice, complete full-rank representations might only exist if the class of discriminators is very powerful or the class of generators is limited. Especially the second part of Assumption III'' might be hard to satisfy in practice. Moreover, finding such representations might be much harder than finding equilibria for the regularized GAN-training dynamics from Section 4.

Nonetheless, we have the following convergence result for GANs that allow for complete full-rank representations:

Theorem E.3. Assume Assumption I', Assumption II and III' hold for (θ^*, ψ^*) . For small enough learning rates, simultaneous and alternating gradient descent for the (unregularized) gradient vector field v are both convergent to $\mathcal{M}_G \times \mathcal{M}'_D$ in a neighborhood of (θ^*, ψ^*) . Moreover, the rate of convergence is at least linear.

Proof (Sketch). The proof is again similar to the proof of Theorem 4.1. We again introduce local coordinates and

¹²Note that \mathcal{M}'_D is a \mathcal{C}^1 -manifold by definition in this setup.

show that for w not in the tangent space of \mathcal{M}'_D at ψ^* , we have $w^\top K_{DD} w < 0$. To see this, note that w must have a nonzero ψ_1 component if it is not in the tangent space of \mathcal{M}'_D at ψ^* . However, using (111), we see that the submatrix of K_{DD} corresponding to the ψ_1 coordinates is given by

$$\tilde{K}_{DD} = 2f''(0) \mathbb{E}_{p_D(x)} [\eta_{\psi_2^*}(x) \eta_{\psi_2^*}(x)^\top]. \quad (150)$$

This matrix is negative definite by Assumption II and the first part of Assumption III''.

Moreover, by applying (112), we see that the component of $K_{DG}w$, $w \in \mathbb{R}^n$, corresponding to the ψ_1 coordinates is given by

$$\partial_w g(\theta^*) = f'(0) \nabla_\theta \mathbb{E}_{p_\theta(x)} [\eta_{\psi_2^*}(x)] |_{\theta=\theta^*} w. \quad (151)$$

Using the second part of Assumption III'', we therefore see that for w not in the tangent space of \mathcal{M}_G at θ^* , we have $K_{DG}w \neq 0$.

The rest of the proof is the same as the proof of Theorem 4.1. \square

For the Dirac-GAN from Section 2, we can obtain a complete full-rank representation, when we parameterize the discriminator D_ψ as $D_\psi(x) = \psi \exp(x)$, i.e. if we set $\psi_1 := \psi$ and $\eta_{\psi_2}(x) := \exp(x)$. It is easy to check that η_{ψ_2} indeed defines a complete full-rank representation and that the Dirac-GAN is locally convergent to $(\theta^*, \psi^*) = (0, 0)$ for this parameterization of $D_\psi(x)$.

F. Experiments

In this section, we describe additional experiments and give more details on our experimental setup. If not noted otherwise, we always use the nonsaturating GAN-objective introduced by Goodfellow et al. (2014) for training the generator. For WGAN-GP we use the generator and discriminator objectives introduced by Gulrajani et al. (2017).¹³

2D-Problems For the 2D-problems, we run unregularized GAN training, R_1 -regularized and R_2 -regularized GAN training as well WGAN-GP with 1 and 5 discriminator update per generator update. We run each method on 4 different 2D-examples for 6 different GAN architectures. The 4 data-distributions are visualized in Figure 8. All 6 GAN architectures consist of 4-layer fully connected neural networks for both the generator and discriminator, where we select the number of hidden units from $\{8, 16, 32\}$ and use select either leaky RELUs (i.e. $\varphi(t) = \max(t, 0.2t)$) or Tanh-activation functions.

¹³The code to reproduce the experiments presented in this section can be found under https://github.com/LMescheder/GAN_stability.

For each method, we try both Stochastic Gradient Descent (SGD) and RMS-Prop with 4 different learning rates: for SGD, we select the learning rate from $\{5 \cdot 10^{-3}, 10^{-2}, 2 \cdot 10^{-2}, 5 \cdot 10^{-2}\}$. For RMSProp, we select it from $\{5 \cdot 10^{-5}, 10^{-4}, 2 \cdot 10^{-4}, 5 \cdot 10^{-4}\}$. For the R_1 -, R_2 - and WGAN-GP-regularizers we try the regularization parameters $\gamma = 1, \gamma = 3$ and $\gamma = 10$. For each method and architecture, we pick the hyperparameter setting which achieves the lowest Wasserstein-1-distance to the true data distribution. We train all methods for 50k iterations and we report the Wasserstein-1-distance averaged over the last 10k iterations. We estimate the Wasserstein-1-distance using the Python Optimal Transport package¹⁴ by drawing 2048 samples from both the generator distribution and the true data distribution.

The best solution found by each method for the “Circle”-distribution is shown in Figure 9. We see that the R_1 - and R_2 -regularizers converge to solutions for which the discriminator is 0 in a neighborhood of the true data distribution. On the other hand, unregularized training and WGAN-GP converge to *energy solutions* where the discriminator forms a potential function for the true data distribution. Please see Section E.1 for details.

CIFAR-10 To test our theory on real-world tasks, we train a DC-GAN architecture (Radford et al., 2015) with 3 convolutional layers and no batch-normalization on the CIFAR-10 dataset (Krizhevsky & Hinton, 2009). We apply different regularization strategies to stabilize the training. To compare the different regularization strategies, we measure the inception score (Salimans et al., 2016) over Wall-clock-time. We implemented the network in the Tensorflow framework (Abadi et al., 2016). For all regularization techniques, we use the RMSProp optimizer (Tieleman & Hinton, 2012) with $\alpha = 0.9$ and a learning rate of 10^{-4} .

For the R_1 and R_2 regularizers from Section 4.1 we use a regularization parameter of $\gamma = 10$. For the WGAN-GP regularizer we also use a regularization parameter of $\gamma = 10$ as suggested by Gulrajani et al. (2017). We train all methods using 1 discriminator update per generator update except for WGAN-GP, for which we try both 1 and 5 discriminator updates

The inception score over time for the different regularization strategies is shown in Figure 6. As predicted by our theory, we see that the R_1 - and R_2 -regularizers from Section 4.1 lead to stable training whereas unregularized GAN training is not stable. We also see that WGAN-GP with 1 or 5 discriminator updates per generator update lead to similar final inception scores on this architecture. The good behavior of WGAN-GP is surprising considering the fact that it does not even converge locally for the Dirac-GAN. One possible

¹⁴<http://pot.readthedocs.io>

explanation is that WGAN-GP oscillates in narrow circles around the equilibrium which might be enough to produce images of sufficiently high quality. Another possible explanation is that WGAN-GP converges to an energy or full-rank solution (Section E) for this example.

Imagenet In this experiment, we use the R_1 -regularizer to learn a generative model of all 1000 Imagenet (Russakovsky et al., 2015) classes at resolution 128×128 in a single GAN. Because of the high variability of this dataset, this is known to be a challenging task and only few prior works have managed to obtain recognizable samples for this dataset. Prior works that report results for this dataset either show a high amount of mode collapse (Salimans et al., 2016; Odena et al., 2017), report results only at a lower resolution (Hjelm et al., 2017) or use advanced normalization layers to stabilize the training (Miyato et al., 2018).

For the Imagenet experiment, we use ResNet-architectures¹⁵ for the generator and discriminator, both having 26 layers in total. Both the generator and discriminator are conditioned on the labels of the input data. The architectures for the generator and discriminator are shown in Table 3. We use pre-activation ResNet-blocks and Leaky RELU-nonlinearities everywhere. We also multiply the output of the ResNet blocks with 0.1. For the generator, we sample a latent variable z from a 256-dimensional unit Gaussian distribution and concatenate it with a 256 dimensional embedding of the labels, which we normalize to the unit sphere. The resulting 512-dimensional vector is then fed into the first fully connected layer of the generator. The discriminator takes as input an image and outputs a 1000 dimensional vector. Depending on the label of the input, we select the corresponding index in this vector and use it as the logits for the GAN-objective.

For training, we use the RMSProp optimizer with $\alpha = 0.99$, $\epsilon = 10^{-8}$ and an initial learning rate of 10^{-4} . We use a batch size of 128 and we train the networks on 4 GeForce GTX 1080 Ti GPUs for 500.000 iterations. Similarly to prior work (Karras et al., 2017; Yazici et al., 2018; Gidel et al., 2018), we use an exponential moving average¹⁶ with decay 0.999 over the weights to produce the final model.

We find that while training this GAN without any regularization quickly leads to mode collapse, using the R_1 -regularizers from Section 4.1 leads to stable training.

¹⁵We used more complicated architectures for the generator and discriminator in an earlier version of this manuscript. The simplified architectures presented in this version are more efficient and perform slightly better.

¹⁶In an earlier version of this manuscript, we instead annealed the learning rate which has a similar effect. However, taking a moving average introduces fewer hyperparameters and led to higher inception scores in our experiments.

Some random (unconditional) samples can be seen in Figure 10. Moreover, Figure 11 and Figure 12 show conditional samples for some selected Imagenet classes. While not completely photorealistic, we find that our model can produce convincing samples from all 1000 Imagenet classes.

We also compare the R_1 -regularizer with WGAN-GP (with 1 discriminator update per generator update). For this comparison, we did not use the exponential moving average over the weights and also did not normalize the embeddings of the labels to the unit sphere. The resulting inception score¹⁷ over the number of iterations is visualized in Figure 7. We find that for this dataset and architecture we can achieve higher inception scores when using the R_1 -regularizer in place of the WGAN-GP regularizer.

celebA and LSUN To see if the R_1 -regularizers helps to train GANs for high-resolution image distributions, we apply our method to the celebA dataset (Liu et al., 2015) and to 4 subsets of the LSUN dataset (Yu et al., 2015) with resolution 256×256 . We use a similar training setup as for the Imagenet experiment, but we use a slightly different architecture (Table 4). As in the Imagenet-experiment, we use preactivation ResNet-blocks and Leaky RELU-nonlinearities everywhere and we multiply the output of the ResNet-blocks with 0.1. We implemented the network in the PyTorch framework and use the RMSProp optimizer with $\alpha = 0.99$ and a learning rate of 10^{-4} . We again found that results can be (slightly) improved by using an exponential moving average with decay 0.999 over the weights to produce the final models. As a regularization term, we use the R_1 -regularizer with $\gamma = 10$. For the latent code z , we use a 256 dimensional Gaussian distribution. The batch size is 64. We trained each model for about 300.000 iterations on 2 GeForce GTX 1080 Ti GPUs.

We find that the R_1 -regularizer successfully stabilizes training of this architecture. Some random samples can be seen in Figures 13, 14, 15, 16 and 17.

celebA-HQ In addition to the generative model for celebA with resolution 256×256 , we train a GAN on the celebA-HQ dataset (Karras et al., 2017) with resolution 1024×1024 . We use almost the same architecture as for celebA (Table 4), but add two more levels to increase the resolution from 256×256 to 1024×1024 and decrease the number of features from 64 to 16. Because of memory constraints, we also decrease the batch size to 24. As in the previous experiments, we use an exponential moving average with decay 0.999 over the weights to produce the final model. In contrast to Karras et al. (2017), we train our model end-to-end during the whole course of training, i.e. we do not

¹⁷For measuring the inception score, we use the public implementation from <http://github.com/sbarratt/inception-score-pytorch>.

use progressively growing GAN-architectures (nor any of the other techniques used by Karras et al. (2017) to stabilize the training). We trained the model for about 300.000 iterations on 4 GeForce GTX 1080 Ti GPUs. We find that the simple R_1 -regularizer stabilizes the training, allowing our model to converge to a good solution without using a progressively growing GAN. Some random samples are shown in Figure 18.

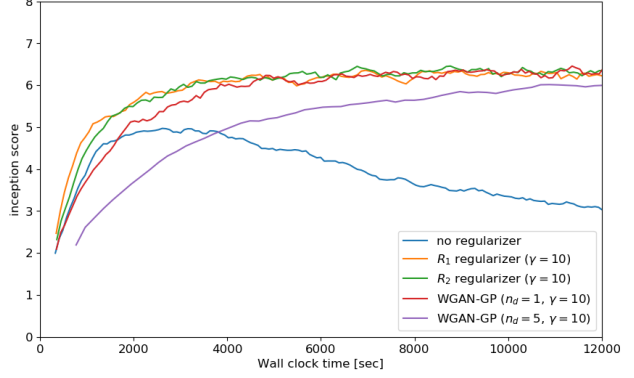


Figure 6. Inception score over time for various regularization strategies when training on CIFAR-10. While the inception score can be problematic for evaluating probabilistic models (Barratt & Sharma, 2018), it still gives a rough idea about the convergence and stability properties of different training methods.

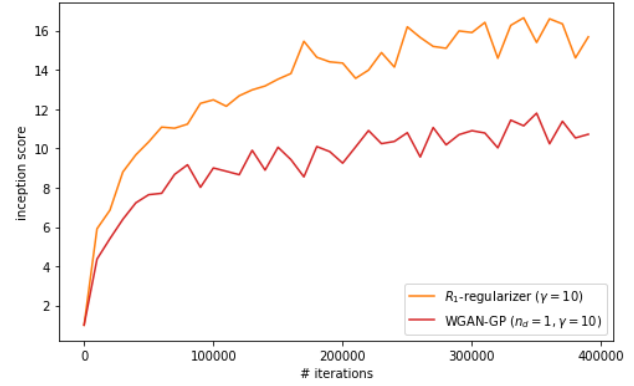


Figure 7. Inception score over the number of iterations for GAN training with R_1 - and WGAN-GP-regularization when training on Imagenet. We find that R_1 -regularization leads to higher inception scores for this dataset and GAN-architecture.

Layer	output size	filter
Fully Connected	$256 \cdot 4 \cdot 4$	$256 \rightarrow 256 \cdot 4 \cdot 4$
Reshape	$256 \times 4 \times 4$	-
TransposedConv2D	$128 \times 8 \times 8$	$256 \rightarrow 128$
TransposedConv2D	$64 \times 16 \times 16$	$128 \rightarrow 64$
TransposedConv2D	$3 \times 32 \times 32$	$64 \rightarrow 3$

(a) Generator architecture

Layer	output size	filter
Conv2D	$64 \times 16 \times 16$	$3 \rightarrow 64$
Conv2D	$128 \times 8 \times 8$	$64 \rightarrow 128$
Conv2D	$256 \times 4 \times 4$	$128 \rightarrow 256$
Reshape	$256 \cdot 4 \cdot 4$	-
Fully Connected	$256 \cdot 4 \cdot 4$	$256 \cdot 4 \cdot 4 \rightarrow 1$

(b) Discriminator architecture

Table 2. Architectures for CIFAR-10-experiment.

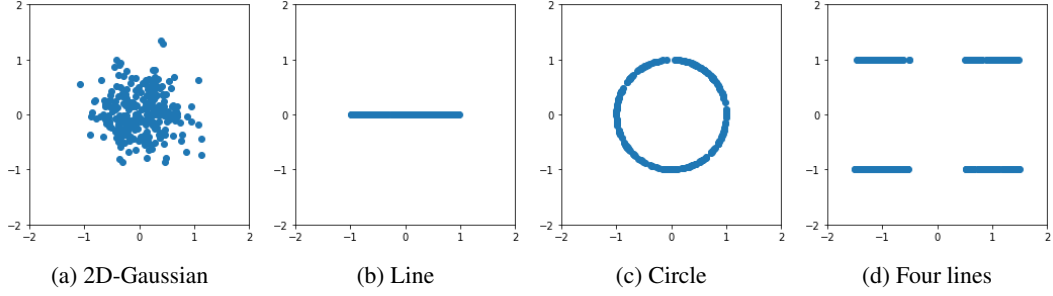


Figure 8. The four 2D-data distributions on which we test the different algorithms.

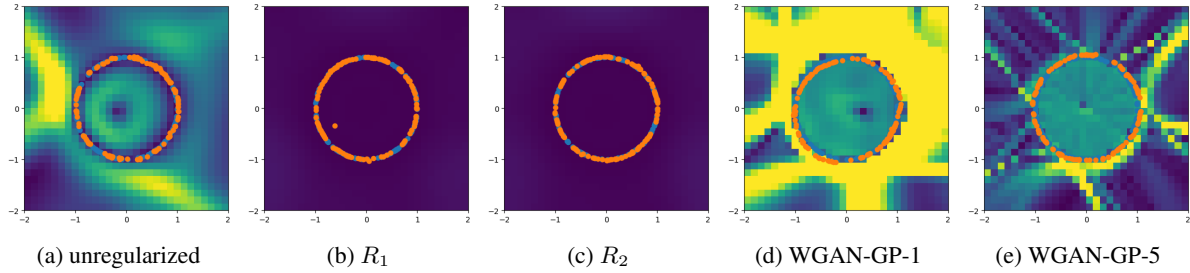


Figure 9. Best solutions found by the different algorithms for learning a circle. The blue points are samples from the true data distribution, the orange points are samples from the generator distribution. The colored areas visualize the gradient magnitude of the equilibrium discriminator. We find that while the R_1 - and R_2 -regularizers converge to equilibrium discriminators that are 0 in a neighborhood of the true data distribution, unregularized training and WGAN-GP converge to energy solutions (Section E.1).

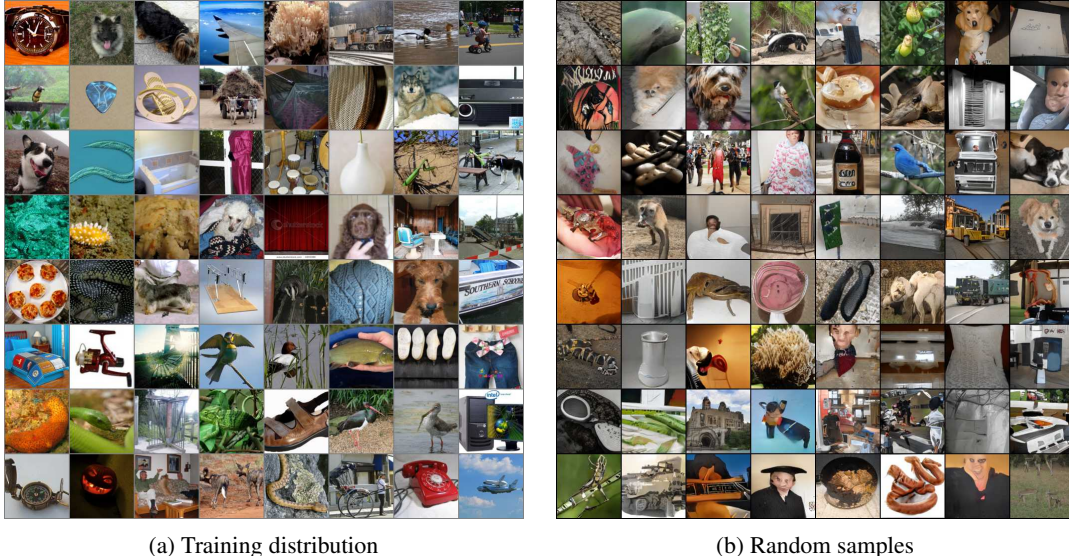


Figure 10. Unconditional random samples for a GAN trained on the ILSVRC dataset (Russakovsky et al., 2015) with resolution 128×128 . The final inception score is 30.2 ± 0.5 .

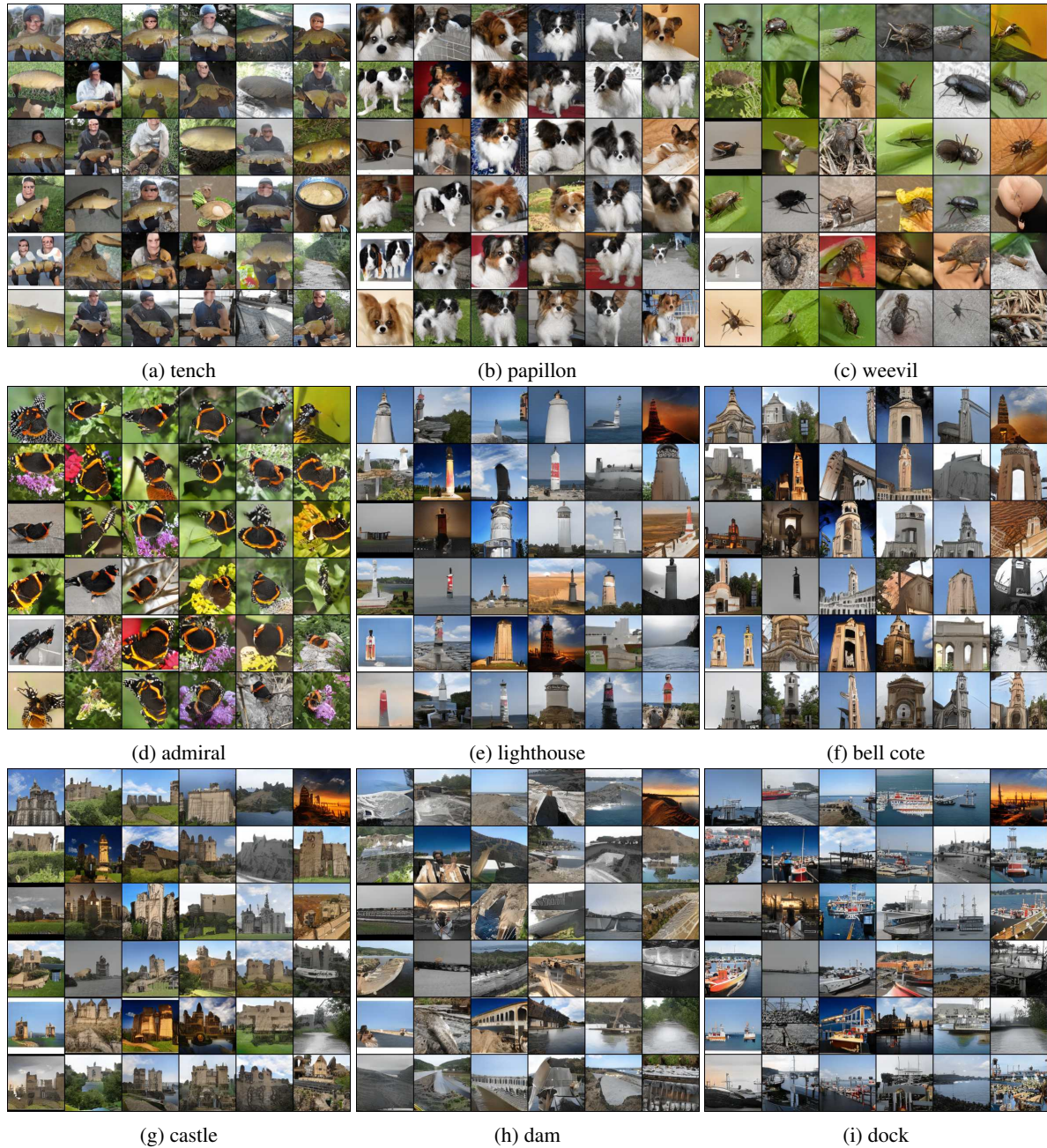


Figure 11. Class conditional random samples for a GAN trained on the Imagenet dataset.

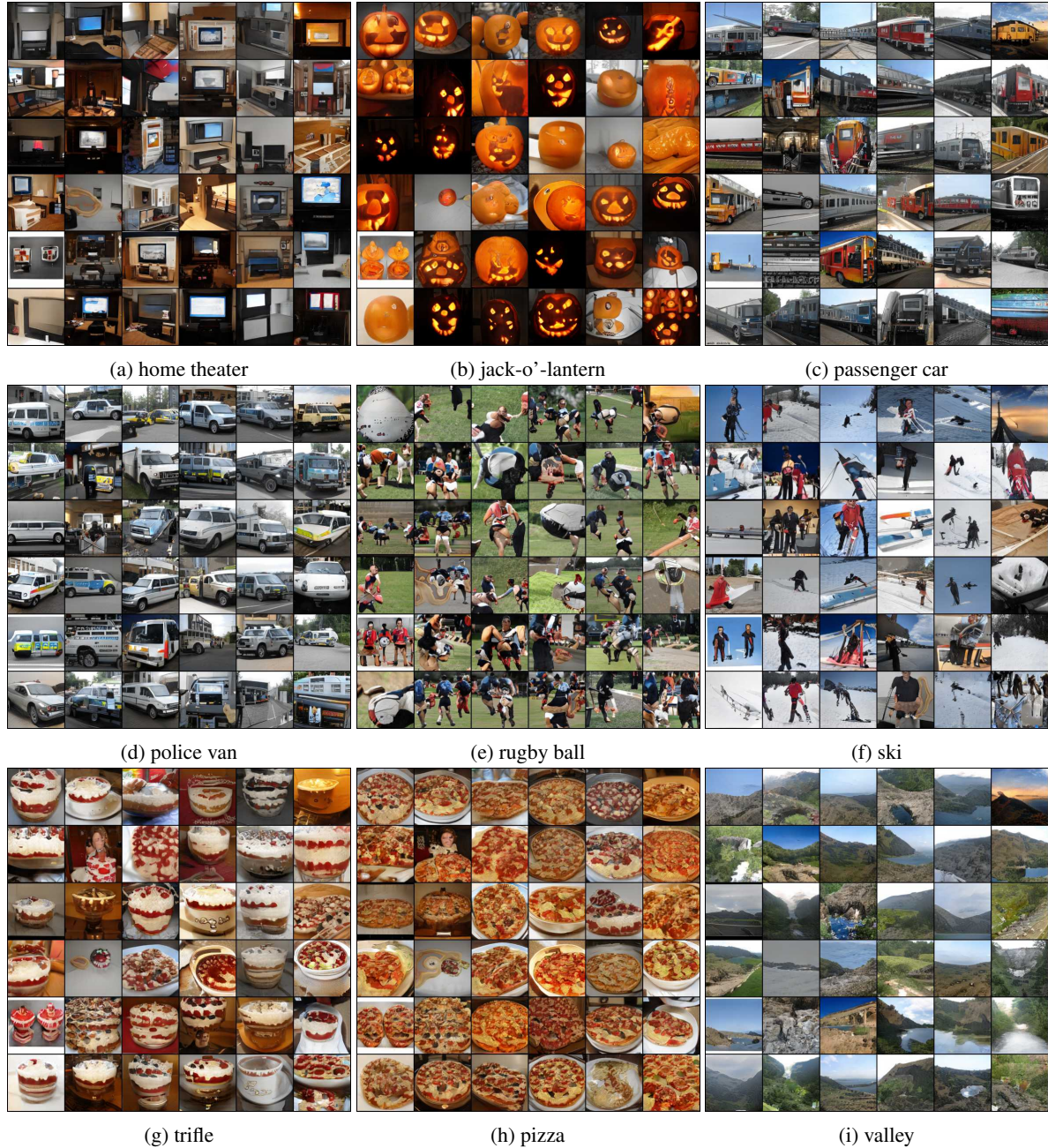


Figure 12. Class conditional random samples for a GAN trained on the Imagenet dataset.



Figure 13. Random samples for a GAN trained on the celebA dataset (Liu et al., 2015) (256×256) for a DC-GAN (Radford et al., 2015) based architecture with additional residual connections (He et al., 2016). For both the generator and the discriminator, we do not use batch normalization.

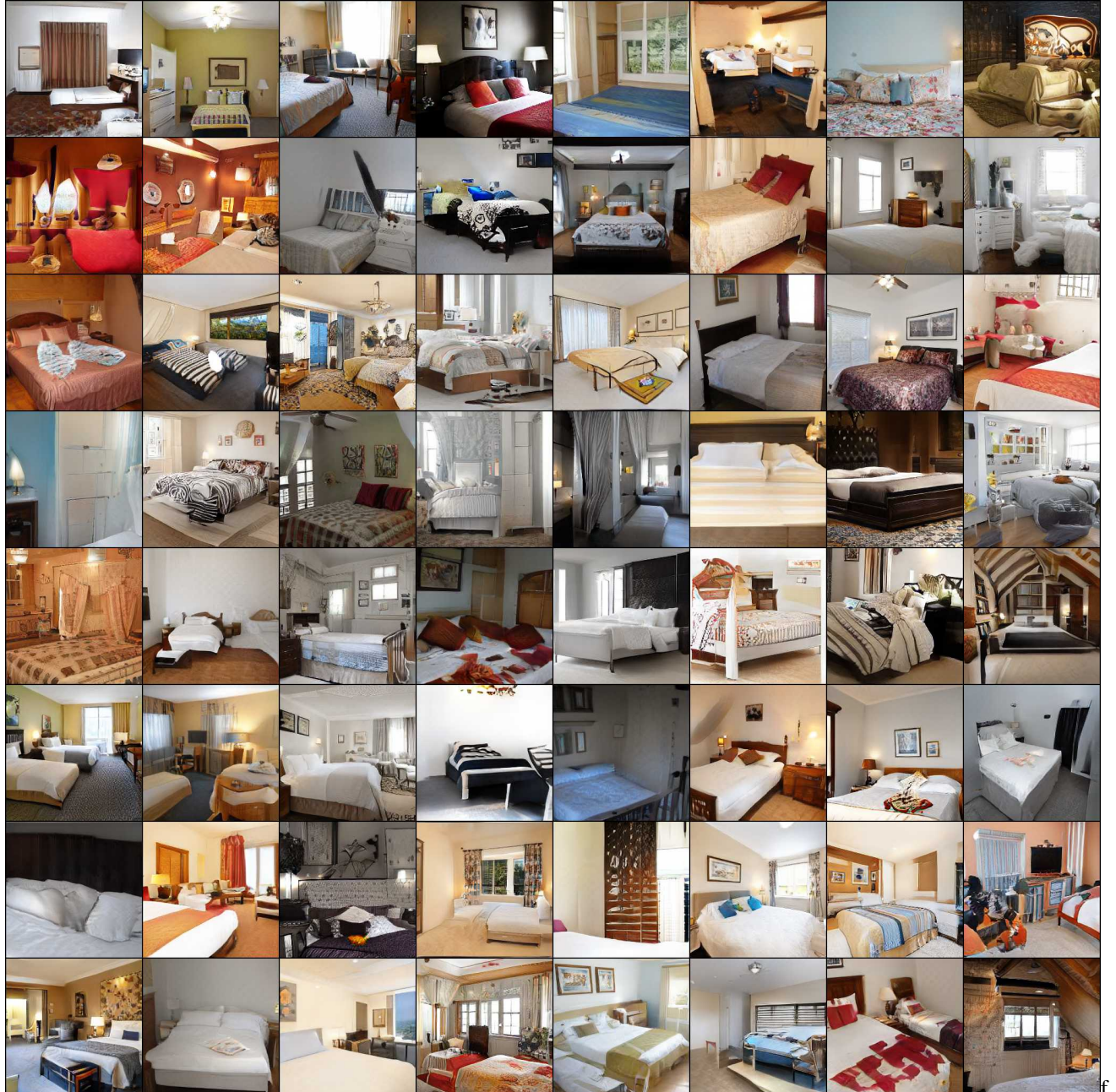


Figure 14. Random samples for a GAN trained on the LSUN-bedroom dataset (Yu et al., 2015) (256×256) for a DC-GAN (Radford et al., 2015) based architecture with additional residual connections (He et al., 2016). For both the generator and the discriminator, we do not use batch normalization.



Figure 15. Random samples for a GAN trained on the LSUN-church dataset (Yu et al., 2015) (256×256) for a DC-GAN (Radford et al., 2015) based architecture with additional residual connections (He et al., 2016). For both the generator and the discriminator, we do not use batch normalization.

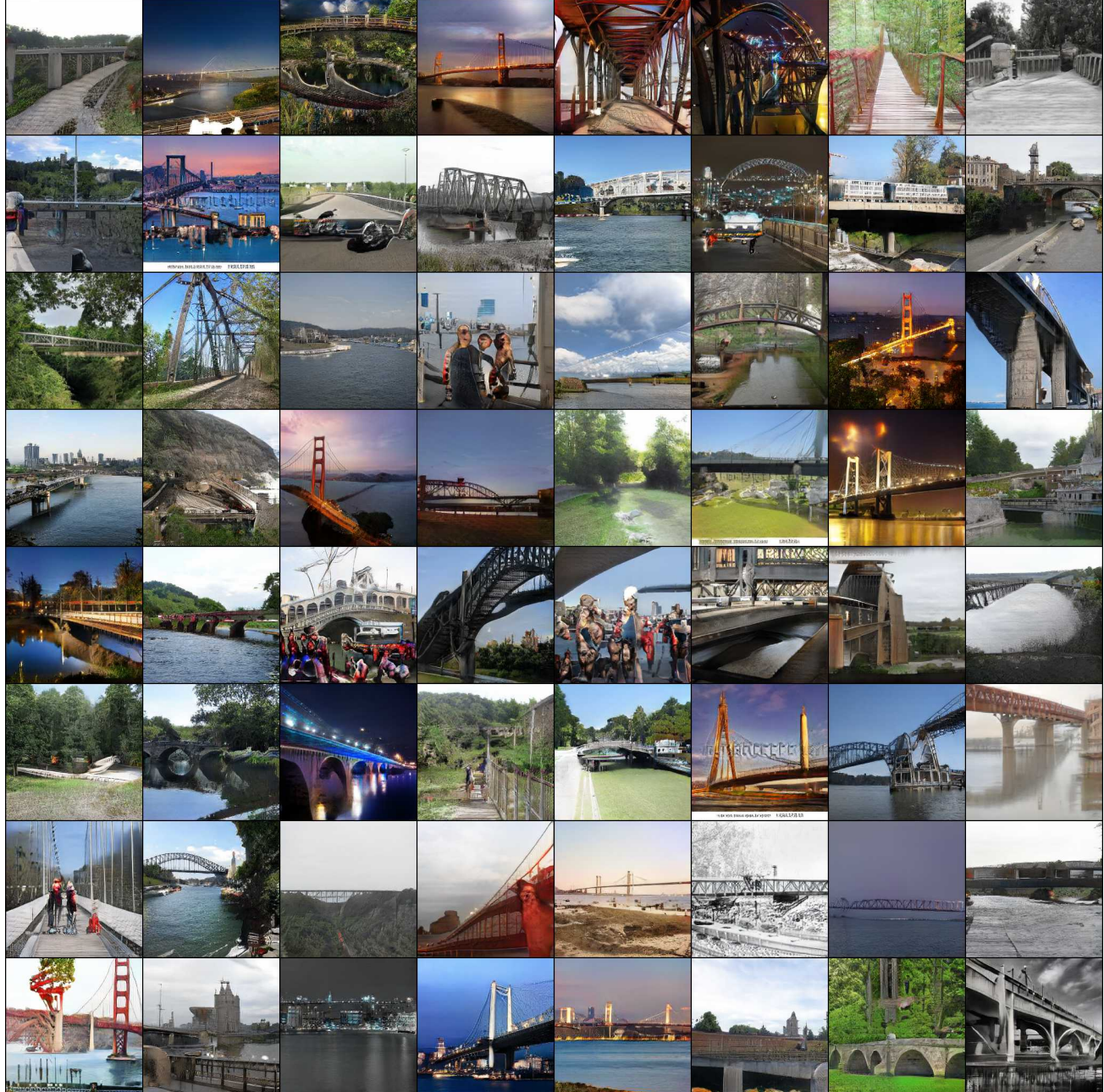


Figure 16. Random samples for a GAN trained on the LSUN-bridge dataset (Yu et al., 2015) (256×256) for a DC-GAN (Radford et al., 2015) based architecture with additional residual connections (He et al., 2016). For both the generator and the discriminator, we do not use batch normalization.



Figure 17. Random samples for a GAN trained on the LSUN-tower dataset (Yu et al., 2015) (256×256) for a DC-GAN (Radford et al., 2015) based architecture with additional residual connections (He et al., 2016). For both the generator and the discriminator, we do not use batch normalization.



Figure 18. Random samples for a GAN trained on the celebA-HQ dataset (Karras et al., 2017) (1024×1024) for a DC-GAN (Radford et al., 2015) based architecture with additional residual connections (He et al., 2016). During the whole course of training, we directly train the full-resolution generator and discriminator end-to-end, i.e. we do not use any of the techniques described in Karras et al. (2017) to stabilize the training.

Layer	output size	filter
Fully Connected	$1024 \cdot 4 \cdot 4$	$512 \rightarrow 1024 \cdot 4 \cdot 4$
Reshape	$1024 \times 4 \times 4$	-
Resnet-Block	$1024 \times 4 \times 4$	$1024 \rightarrow 1024 \rightarrow 1024$
Resnet-Block	$1024 \times 4 \times 4$	$1024 \rightarrow 1024 \rightarrow 1024$
NN-Upsampling	$1024 \times 8 \times 8$	-
Resnet-Block	$1024 \times 8 \times 8$	$1024 \rightarrow 1024 \rightarrow 1024$
Resnet-Block	$1024 \times 8 \times 8$	$1024 \rightarrow 1024 \rightarrow 1024$
NN-Upsampling	$1024 \times 16 \times 16$	-
Resnet-Block	$512 \times 16 \times 16$	$1024 \rightarrow 512 \rightarrow 512$
Resnet-Block	$512 \times 16 \times 16$	$512 \rightarrow 512 \rightarrow 512$
NN-Upsampling	$512 \times 32 \times 32$	-
Resnet-Block	$256 \times 32 \times 32$	$512 \rightarrow 256 \rightarrow 256$
Resnet-Block	$256 \times 32 \times 32$	$256 \rightarrow 256 \rightarrow 256$
NN-Upsampling	$256 \times 64 \times 64$	-
Resnet-Block	$128 \times 64 \times 64$	$256 \rightarrow 128 \rightarrow 128$
Resnet-Block	$128 \times 64 \times 64$	$128 \rightarrow 128 \rightarrow 128$
NN-Upsampling	$128 \times 128 \times 128$	-
Resnet-Block	$64 \times 128 \times 128$	$128 \rightarrow 64 \rightarrow 64$
Resnet-Block	$64 \times 128 \times 128$	$64 \rightarrow 64 \rightarrow 64$
Conv2D	$3 \times 128 \times 128$	$64 \rightarrow 3$

(a) Generator architecture

Layer	output size	filter
Conv2D	$64 \times 128 \times 128$	$3 \rightarrow 64$
Resnet-Block	$64 \times 128 \times 128$	$64 \rightarrow 64 \rightarrow 64$
Resnet-Block	$128 \times 128 \times 128$	$64 \rightarrow 64 \rightarrow 128$
Avg-Pool2D	$128 \times 64 \times 64$	-
Resnet-Block	$128 \times 64 \times 64$	$128 \rightarrow 128 \rightarrow 128$
Resnet-Block	$256 \times 64 \times 64$	$128 \rightarrow 128 \rightarrow 256$
Avg-Pool2D	$256 \times 32 \times 32$	-
Resnet-Block	$256 \times 32 \times 32$	$256 \rightarrow 256 \rightarrow 256$
Resnet-Block	$512 \times 32 \times 32$	$256 \rightarrow 256 \rightarrow 512$
Avg-Pool2D	$512 \times 16 \times 16$	-
Resnet-Block	$512 \times 16 \times 16$	$512 \rightarrow 512 \rightarrow 512$
Resnet-Block	$1024 \times 16 \times 16$	$512 \rightarrow 512 \rightarrow 1024$
Avg-Pool2D	$1024 \times 8 \times 8$	-
Resnet-Block	$1024 \times 8 \times 8$	$1024 \rightarrow 1024 \rightarrow 1024$
Resnet-Block	$1024 \times 8 \times 8$	$1024 \rightarrow 1024 \rightarrow 1024$
Avg-Pool2D	$1024 \times 4 \times 4$	-
Resnet-Block	$1024 \times 4 \times 4$	$1024 \rightarrow 1024 \rightarrow 1024$
Resnet-Block	$1024 \times 4 \times 4$	$1024 \rightarrow 1024 \rightarrow 1024$
Fully Connected	$1024 \cdot 4 \cdot 4$	$1024 \cdot 4 \cdot 4 \rightarrow 1000$

(b) Discriminator architecture

Layer	output size	filter
Fully Connected	$1024 \cdot 4 \cdot 4$	$512 \rightarrow 1024 \cdot 4 \cdot 4$
Reshape	$1024 \times 4 \times 4$	-
Resnet-Block	$1024 \times 4 \times 4$	$1024 \rightarrow 1024 \rightarrow 1024$
NN-Upsampling	$1024 \times 8 \times 8$	-
Resnet-Block	$1024 \times 8 \times 8$	$1024 \rightarrow 1024 \rightarrow 1024$
NN-Upsampling	$1024 \times 16 \times 16$	-
Resnet-Block	$512 \times 16 \times 16$	$1024 \rightarrow 512 \rightarrow 512$
NN-Upsampling	$512 \times 32 \times 32$	-
Resnet-Block	$256 \times 32 \times 32$	$512 \rightarrow 256 \rightarrow 256$
NN-Upsampling	$256 \times 64 \times 64$	-
Resnet-Block	$128 \times 64 \times 64$	$256 \rightarrow 128 \rightarrow 128$
NN-Upsampling	$128 \times 128 \times 128$	-
Resnet-Block	$64 \times 128 \times 128$	$128 \rightarrow 64 \rightarrow 64$
NN-Upsampling	$64 \times 256 \times 256$	-
Resnet-Block	$64 \times 256 \times 256$	$64 \rightarrow 64 \rightarrow 64$
Conv2D	$3 \times 256 \times 256$	$64 \rightarrow 3$

(a) Generator architecture

Layer	output size	filter
Conv2D	$64 \times 256 \times 256$	$3 \rightarrow 64$
Resnet-Block	$64 \times 256 \times 256$	$64 \rightarrow 64 \rightarrow 64$
Avg-Pool2D	$64 \times 128 \times 128$	-
Resnet-Block	$128 \times 128 \times 128$	$64 \rightarrow 64 \rightarrow 128$
Avg-Pool2D	$128 \times 64 \times 64$	-
Resnet-Block	$256 \times 64 \times 64$	$128 \rightarrow 128 \rightarrow 256$
Avg-Pool2D	$256 \times 32 \times 32$	-
Resnet-Block	$512 \times 32 \times 32$	$256 \rightarrow 256 \rightarrow 512$
Avg-Pool2D	$512 \times 16 \times 16$	-
Resnet-Block	$1024 \times 16 \times 16$	$512 \rightarrow 512 \rightarrow 1024$
Avg-Pool2D	$1024 \times 8 \times 8$	-
Resnet-Block	$1024 \times 8 \times 8$	$1024 \rightarrow 1024 \rightarrow 1024$
Avg-Pool2D	$1024 \times 4 \times 4$	-
Fully Connected	$1024 \cdot 4 \cdot 4$	$1024 \cdot 4 \cdot 4 \rightarrow 1$

(b) Discriminator architecture

Table 4. Architectures for LSUN- and celebA-experiments.

Table 3. Architectures for Imagenet-experiment.

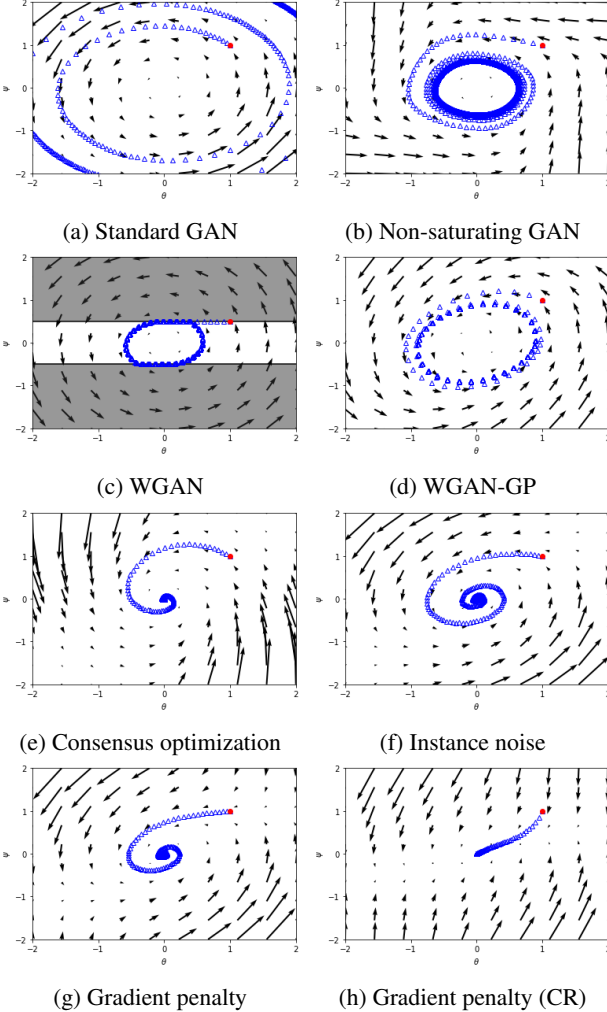


Figure 19. Convergence properties of different GAN training algorithms using simultaneous gradient descent. The shaded area in Figure 19c visualizes the set of forbidden values for the discriminator parameter ψ . The starting iterate is marked in red.

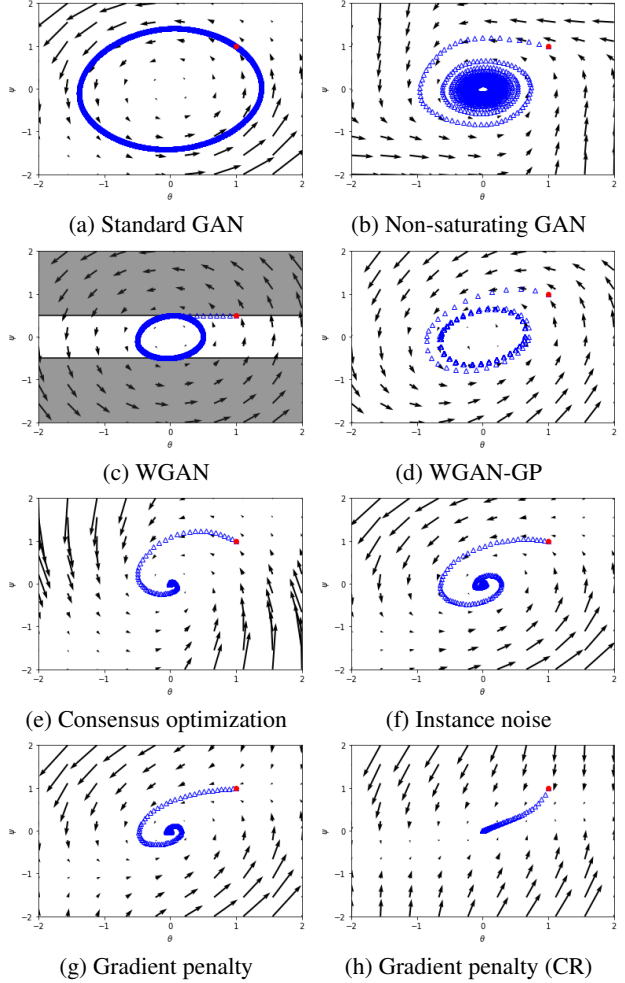


Figure 20. Convergence properties of different GAN training algorithms using alternating gradient descent with 1 discriminator update per generator update. The shaded area in Figure 20c visualizes the set of forbidden values for the discriminator parameter ψ . The starting iterate is marked in red.

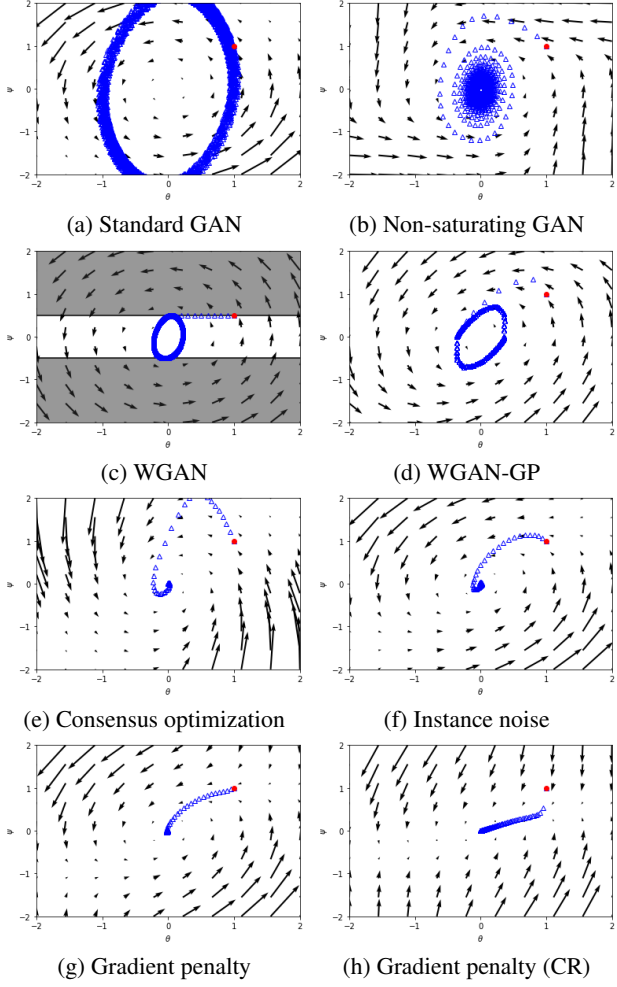


Figure 21. Convergence properties of different GAN training algorithms using alternating gradient descent with 5 discriminator updates per generator update. The shaded area in Figure 21c visualizes the set of forbidden values for the discriminator parameter ψ . The starting iterate is marked in red.

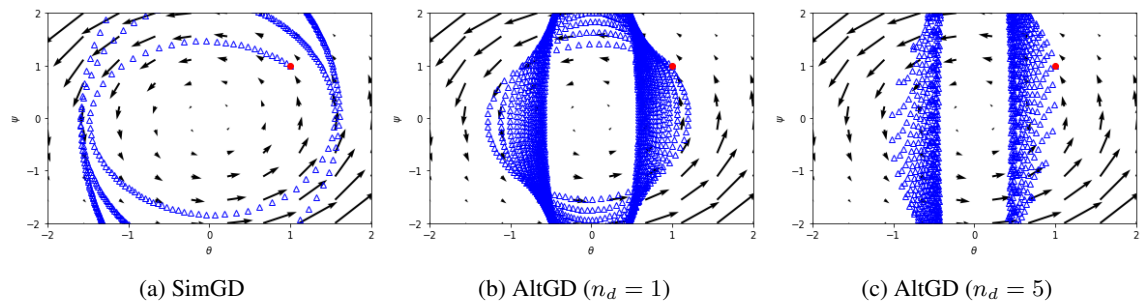


Figure 22. Convergence properties of our GAN using two time-scale training as proposed by Heusel et al. (2017). For the Dirac-GAN we do not see any sign of convergence when training with two time-scales. The starting iterate is marked in red.